Using M_{T2} to distinguish dark matter stabilization symmetries

Kaustubh Agashe, Doojin Kim, Devin G. E. Walker, and Lijun Zhu

Using M_{T2} to Distinguish Dark Matter Stabilization Symmetries

Kaustubh Agashe[1], Doojin Kim[1], Devin G. E. Walker[2] and Lijun Zhu[1]

[1]*Maryland Center for Fundamental Physics, Department of Physics, University of Maryland, College Park, Maryland 20742, U. S. A.*

and

[2]*Center for the Fundamental Laws of Nature, Jefferson Physical Laboratory, Harvard University, Cambridge, Massachusetts 02138, U. S. A.*

Abstract

We examine the potential of using colliders to distinguish models with parity (Z_2) stabilized dark matter (DM) from models in which the DM is stabilized by other symmetries, taking the latter to be a Z_3 symmetry for illustration. The key observation is that a heavier mother particle charged under a Z_3 stabilization symmetry can decay into *one or two* DM particles along with Standard Model (SM) particles. This can be contrasted with the decay of a mother particle charged under a parity symmetry; typically, only one DM particle appears in the decay chain. The arXiv:1003.0899 studied the distributions of *visible* invariant mass from the decay of a *single* such mother particle in order to highlight the resulting distinctive signatures of Z_3 symmetry versus parity symmetry stabilized dark matter candidates. We now describe a complementary study which focuses on decay chains of the *two* mother particles which are necessarily present in these events. We also include in our analyss the *missing* energy/momentum in the event. For the Z_3 symmetry stabilized mothers, the resulting inclusive final state can have two, three or four DM particles. In contrast, models with Z_2 symmetry can have only two. We show that the shapes and edges of the distribution of M_{T2}-type variables, along with ratio of the visible momentum/energy on the two sides of the event, are powerful in distinguishing these different scenarios. Finally we conclude by outlining future work which focus on reducing combinatoric ambiguities from reconstructing multi-jet events. Increasing the reconstruction efficiency can allow better reconstruction of events with two or three dark matter candidates in the final state.

1   Introduction

A stable weakly interacting massive particle (WIMP) – with a mass also of order the weak scale – is a well-motivated candidate for dark matter (DM) in the universe since it approximately has the correct relic density upon thermal freeze-out [1]. Such a particle also often arises in extensions of the Standard Model (SM), especially those motivated by solutions to the Planck-weak hierarchy problem of the SM. Finally, if the WIMP is a part of an extension of the SM, then it is likely to have (weak) interactions with SM particles. Hence, the WIMP paradigm can be tested via *non-gravitational* methods, for example, direct/indirect detection of cosmic DM or production of the DM at colliders. The latter is our interest here.

The collider searches of the DM paradigm typically involve producing a *heavier* particle charged under the same symmetry which stabilizes the DM. Such a "mother" particle must decay to SM particles and DM, manifesting as missing energy, along with a SM final state. Reconstructing the decay chains leading to such events will enable us to determine the masses of the DM and the mother particles; it is advantageous to do this in a model-*independent* manner. A tremendous amount of effort has been put-in into such a research program, especially at the CERN Large Hadron Collider (LHC), see, for example [2, 3, 4, 5, 6, 7, 8, 9, 10, 11, 12, 13, 14, 15, 16, 17, 18, 19, 20, 21, 22]. See also [23] for a review. Most of this work still assumes that a Z_2/parity symmetry stabilizes the DM (henceforth called Z_2 models). This is partly because there are several models with such a symmetry [25, 26, 27, 28, 29]. However, while Z_2 might be the simplest possibility for such a symmetry, it is by no means the only one [30, 33, 32, 34]. So, in previous work [31, 36], the program of instead *determining* the DM stabilization symmetry from collider data was started. We focused on how to distinguish a Z_3 DM stabilization symmetry (henceforth called a Z_3 model) from a Z_2 model[1]. We have focused on Z_3 models for simplicity and definiteness. However, we emphasize our techniques in this and in previous papers [31, 36] can be generalized to distinguish most other DM stabilization symmetries from parity symmetry stabilized DM.

The basic idea behind distinguishing Z_3 from Z_2 models is that a

- *single* mother charged under a Z_3 symmetry is allowed (based simply on the symmetry) to decay into *one* or *two* DM candidates.

This is to be contrasted with the fact that mother particles charged under a Z_2 symmetry have only *one* DM candidate in the final state[2]. As discussed in reference [36], decays of a *single* Z_3-charged mother particle generate a "double edge" in the invariant mass distribution of the *visible*

---

[1]See reference [35] for how calculation of relic density and indirect detection might be modified in a Z_3 model vs. a Z_2 model. Also see reference [31] for a collider study of non-Z_2 models, but with decays of mother particles into DM occurring *outside* the detector vs. the case of such decays taking place inside the detector studied here and in reference [36].

[2]In both Z_3 and Z_2 models, a mother can decay into *three* DM particles, but we will not consider this possibility here for simplicity and since it is expected to be phase-space suppressed compared to the other possibilities.

(SM) particles. This is with the condition that the intermediate particles in the decay chains are off-shell and that the decay chains with one and two DM contain identical SM particles. For the case of on-shell intermediate particles, it was shown in [36] that this invariant mass distribution has a "cusp" for certain decay topology (with two DM) of a Z_3 mother particle. In all, [36] focused on new features in observables from a single decay chain only.

In this work we consider the total inclusive event in order glean even more information, recalling that there must be two such mother particles present. For example, consider the case where there is only one visible (SM) particle in the decay chain of a mother particle. Constructing the invariant mass of the visible particle of this decay chain, as per the analysis of [36], is not very useful for the purpose of reconstructing the mass of the mother particle: one might have to resort to including information about the invisible particle(s) in the same decay chain. Since we can only measure the *total* missing transverse momentum in the event which is *shared* between invisible particles from two mothers, we must use measurements from both sides. An option is to use "M_{T2}"-type observables/variables [2, 3, 4, 5, 6, 7, 8, 9, 10, 11, 12, 13, 14, 15, 16] Another case where one of the analyses of reference [36] (based on single mother decay) might not work is when the visible/SM particles in the decay chains with one and two DM (of course for Z_3 model) are not identical (even if they are more than one). Thus, one does not obtain a double edge for the case of intermediate particles in the decay chains being *off*-shell.

With the above motivations in mind, in this paper,

- we develop techniques for distinguishing Z_3 models from Z_2 models using information from *both* mother decays and the *missing* (in addition to visible) energy/momentum in an event.

We especially study the above cases where the techniques of reference [36] might not work – in this sense, our present work is *complementary* to that of reference [36].

- We show that shapes and edges of these M_{T2} distributions, along with ratio of visible momentum/energy on the two sides of the event act as powerful discriminants between Z_3 and Z_2 models (including the case of a neutrino, i.e., mass*less* invisible particle – in addition to DM, in the final state for Z_2 models).

An outline of this paper is as follows: In the next section, we begin with a review of M_{T2} variable in Z_2 models. We present some important formulae such as the location of maximum value of the M_{T2} distribution, and discuss some interesting features such as a "kink" in the maximum M_{T2} as a function of the "trial" DM mass in the case where more than one visible particle is involved in each decay chain. In Sec. 3 we move on to the M_{T2} variable in Z_3 models. We define three different event types arising in Z_3 models based on the number of dark matter particles in the final state and provide their corresponding theoretical predictions of the maximum M_{T2}. In particular, we discuss the conditions to have a kink in maximum M_{T2} as a function of trial DM mass for the cases

where there exist more than two DM particles in the final state: such situations do not arise in Z_2 models. We further show some simulation results for M_{T2} distributions for the new types of events in Z_3 models and discuss some notable features to be used for distinguishing Z_3 models from Z_2 models.

In the following two sections, we provide detailed applications of our results of the previous two sections for distinguishing Z_3 from Z_3 models. First we consider the easier case where the decay chain with one DM contains visible/SM particle(s) which are *not* identical to the ones in the two DM decay chain mentioned above (in Z_3 models). Based on the theoretical considerations given in Secs. 2 and 3, we provide ways of distinguishing Z_3 models from Z_2 models, as well as measuring the mother and DM masses. We do it for both the case of one visible/SM particle in the two decay chains and more than one visible/SM particle case. In the next section we deal with the case where one DM and two DM decay chains contain identical visible/SM particle(s), and discuss *additional* techniques required in this case to distinguish Z_2 and Z_3 models. In all of the examples above, we make the simplifying assumption that the intermediate particles in the decay chain are *off*-shell, i.e., they are heavier than the mass of their mother particle. In section 6, we briefly mention some aspects of the case of intermediate particles being on-shell. We next conclude and show details of some of the calculations in the Appendix.

2   A Review of M_{T2} for Z_2 Models

For simplicity, in this paper

- we consider pair-production of a *single* type of mother particle which is charged under the DM stabilization symmetry.

We also assume that the *total* transverse momentum of the two mothers particles produced in an event is zero, for example, we neglect any initial/final state radiation. In Z_2 models, each such mother decays into SM/visible particle(s) and one DM/invisible particle[3]. Furthermore, it is assumed

- we know which *visible* particle(s) originate from which decay chain.[4] For example, if the pair-produced mother particles are boosted sufficiently, their decay products are likely to be collimated so that the visible particles coming from the same decay chain are detected in the same hemisphere in the collider. For alternate methods of determining the correct assignment of visible particles to the two decay chains, see reference [37] and section 6.3.

---

[3]We assume that there is only one type of DM particle in this (and similarly the Z_3) model so that the invisible/DM particles in each decay chain are identical.

[4]Of course, for Z_3 models, we do not know which decay chain emits one or two DM particles.

The M_{T2} variable [2, 3] is a generalization of the transverse mass[5] to this case. Specifically, for each event, it is defined to be a minimization of the maximum of the two transverse masses in each decay chain under the constraint that the sum of all the transverse momenta of the visible and invisible particles vanishes [2, 3]:

$$M_{T2} \equiv \min_{\mathbf{p}_T^{v(1)} + \mathbf{p}_T^{v(2)} + \tilde{\mathbf{p}}_T^{(1)} + \tilde{\mathbf{p}}_T^{(2)} = 0} \left[\max \left\{ M_T^{(1)}, \, M_T^{(2)} \right\} \right] \tag{1}$$

where $\mathbf{p}_T^{v(i)}$ denote the vector *sum* of visible transverse momenta and $\tilde{\mathbf{p}}_T^{(i)}$ denote the transverse momentum of the invisible particle in the ith decay chain ($i = 1, 2$): the minimization is performed over the latter momenta. $M_T^{(i)}$ is the usual transverse mass:

$$\left(M_T^{(i)} \right)^2 = \left(m_T^{v(i)} \right)^2 + \tilde{m}^2 + 2 \left(E_T^{v(i)} \tilde{E}_T^{(i)} - \mathbf{p}_T^{v(i)} \cdot \tilde{\mathbf{p}}_T^{(i)} \right) \tag{2}$$

where $E_T^{v(i)}$ and $m_T^{v(i)}$ are (respectively) the transverse energy and transverse mass formed by all visible particles belonging to the same decay chain. The variables with a tilde represent the corresponding quantities formed by the invisible particle in the same decay chain. Note that the mass of the invisible particle $\tilde{m}$ should be regarded as a unknown/free parameter because we are not aware of it in advance, and henceforth we call it "trial" DM mass. In this sense M_{T2} should be considered to be a function of the trial DM mass $\tilde{m}$, and its maximum value among many events (which will be used extensively in the following) is defined as

$$M_{T2}^{\max}(\tilde{m}) = \max_{\text{many events}} \left[M_{T2}(\tilde{m}) \right]. \tag{3}$$

Obviously $M_{T2}^{\max}(\tilde{m})$ is also a function of the trial DM mass (see App. A for details). An important result to be noted is that if there are a sufficient number of events and the actual DM mass is substituted into $\tilde{m}$, then the above-given $M_{T2}^{\max}$ becomes the actual mass of the pair-produced mother particles [2, 3]:

$$M_{T2}^{\max}(\tilde{m} = m_{DM}) = M \tag{4}$$

where M and m_{DM} indicate the true masses of mother and DM, respectively.

In order to see how this M_{T2} analysis is applied to realistic situations, we first take the case where there exists a single visible/SM particle in each decay chain, and then move on to the case where there exist more than one visible/SM particle in each decay chain. A similar analysis can be done for mixed case, i.e., one visible particle on one side and more than one on the other.

2.1   One Visible/SM Particle in Each Decay Chain

In this case the upper edge in M_{T2} distribution is obtained by "balanced" [2, 3, 4] solution (see App. A for details).

$$M_{T2}^{\max} = M_{T2}^{\max, bal} = \sqrt{\frac{(M^2 - m_{DM}^2)^2}{4M^2}} + \sqrt{\frac{(M^2 - m_{DM}^2)^2}{4M^2} + \tilde{m}^2} \tag{5}$$

[5]Of course, the usual transverse mass assumes only a single mother particle.

1 visible particle per chain
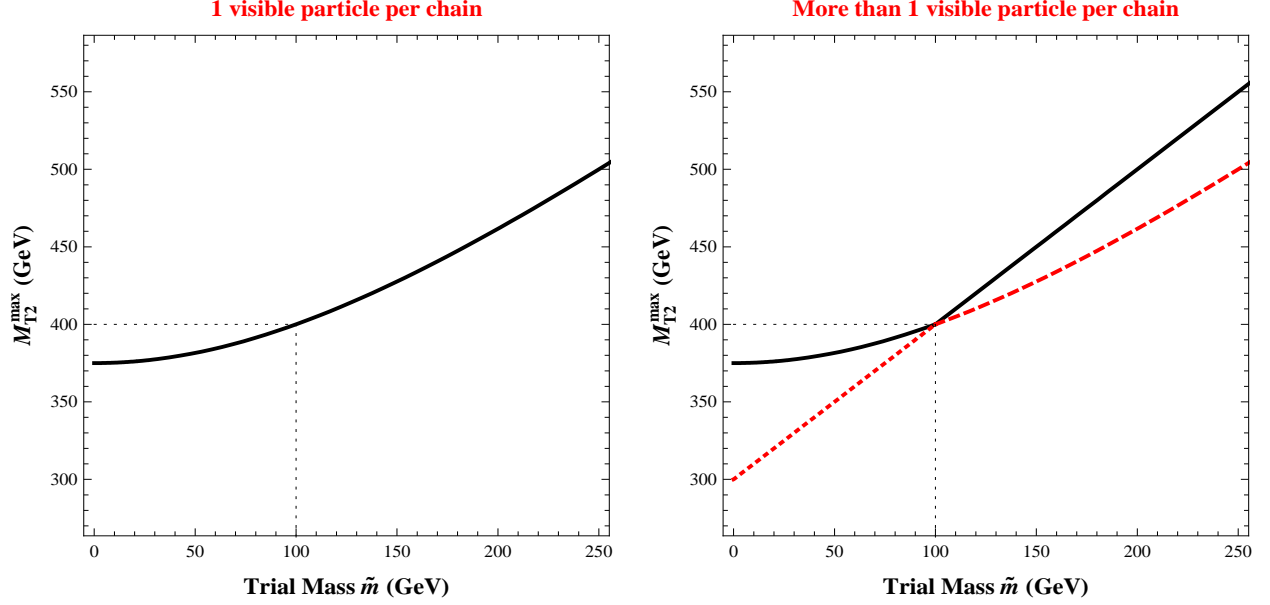
More than 1 visible particle per chain

Figure 1: Theoretical expectation of $M_{T2}^{\max}$ versus the trial mass $\tilde{m}$ for Z_2 events. The masses of mother and DM particles are 400 GeV and 100 GeV, respectively. The left panel shows the case where there exists only a single visible particle per chain. The right panel shows the case where there exist more than one visible particle per decay chain. In both panels, the solid black curve represents the overall/net upper edge, $M_{T2}^{\max}$. In the right panel, the dotted straight line which extends into the right-hand part of the solid line is the $M_{T2}^{\max}$ for the unbalanced solution, whereas the dashed line which extends into the left-hand part of the solid line is that for the balanced solution.

Here (and henceforth)

- we assume that all visible particles are massless for simplicity.

As mentioned earlier, the above-given upper edge is a function of the trial DM mass $\tilde{m}$ and one can see that it reduces to the true mother mass M with $\tilde{m}$ equal to the true DM mass m_{DM}. The left panel of Fig. 1 shows the above theoretical prediction for the location of maximum M_{T2} for Z_2 models as a function of the trial mass $\tilde{m}$. We used 400 GeV and 100 GeV as mother and DM particle masses. As expected from Eq. (5), the curve in the figure "smoothly" increases with $\tilde{m}$ (cf. the following section), and that the $M_{T2}^{\max}$ value corresponding to $\tilde{m} = m_{DM}$ (here 100 GeV) is the same as the true mother particle mass (here 400 GeV: see the black dotted lines).

2.2 More than One Visible/SM Particle in Each Decay Chain

Once there exist more than one visible particle per decay chain, another type of solution to M_{T2}, denoted by "unbalanced" [2, 3, 4], arises. If

- we assume that the intermediate particles in the decay chains are *off*-shell, i.e., heavier than their mother particles

6

(as we will for most of this paper), then the balanced solution in this case is still given by Eq. (5), and the unbalanced solution is as follows[6]:

$$M_{T2}^{\max,unbal} = M - m_{DM} + \tilde{m}. \tag{6}$$

Hence the overall upper edge in the M_{T2} distribution is determined by a "competition" between balanced and unbalanced solutions:

$$M_{T2}^{\max} = \max\left[M_{T2}^{\max,bal}, \ M_{T2}^{\max,unbal}\right] = \begin{cases} M - m_{DM} + \tilde{m} & \text{for } \tilde{m} \geq m_{DM} \\ \sqrt{\frac{(M^2 - m_{DM}^2)^2}{4M^2}} + \sqrt{\frac{(M^2 - m_{DM}^2)^2}{4M^2} + \tilde{m}^2} & \text{for } \tilde{m} \leq m_{DM}. \end{cases} \tag{7}$$

Note that the $M_{T2}^{\max}$ shows different functional behaviors depending on the relative size of the trial DM mass to the true DM mass. As a result, $M_{T2}^{\max}$ is no longer smoothly increasing with $\tilde{m}$ in contrast to the case with one visible/SM per decay chain. Instead, there arises a "kink" at the location of the actual DM mass, with the corresponding $M_{T2}^{\max}$ being the actual mother mass [4][7]. This is illustrated in the right panel of Fig. 1 where the upper edges for the two possible types of solutions $M_{T2}^{\max,unbal}$ and $M_{T2}^{\max,bal}$ are shown by a straight line (i.e., the dotted line, which extends into the right-hand part of the solid line) and a dashed curve (which extends into the left-hand part of the solid curve), respectively. The upper edge in the M_{T2} distribution is given by the larger of these two values, i.e., the black solid curve, and shows a kink (indicated by the black dotted lines), at $\tilde{m} = 100$ GeV and $M_{T2}^{\max} = 400$ GeV (as expected).

3 M_{T2} for Z_3 Models

To begin with, we would like to reiterate some of the relevant features of Z_3 symmetry in order to avoid any possible confusion later. Under the Z_3 symmetry, a particle/field ϕ transforms as

$$\phi \quad \longrightarrow \quad \phi \exp\left(\frac{2\pi i q}{3}\right) \tag{8}$$

where $q = 0$ (i.e., neutral) or $+1$, $+2$. Suppose the lightest of the Z_3 charged particles (labelled ϕ_0) has charge $q = +1$ (similar argument can be made for charge $q = +2$). Clearly, its anti-particle ($\bar{\phi}_0$) has (a different) charge $q = -1$ (which is equivalent to $q = +2$) and has the same mass as ϕ_0. Then, solely based on Z_3 symmetry considerations, all other (heavier) Z_3-charged particles can decay into this lightest Z_3-charged particle or its anti-particle (in addition to Z_3-neutral particles, including SM particles). To be explicit, a heavier Z_3-charged particle with charge $q = +1$ can decay into either (single) ϕ_0 or *two* $\bar{\phi}_0$'s (and Z_3-neutral particles). Taking the CP conjugate of the preceding

---

[6]Of course, in general, one can find the expressions for both the balanced and the unbalanced solutions in the case of *on*-shell intermediate particles [4].

[7]A similar kink also appears for the case of *one* visible particle in each decay chain *if* the total transverse momentum of the two mother particles is *non*-zero, for example, in the presence of initial/final state radiation (see [5]), but (as mentioned earlier) we neglect this possibility for simplicity.

statement, we see that a heavier Z_3-charged particle with the other type of charge, namely $q = 2$, is allowed to decay into *two* ϕ_0's or single $\bar{\phi}_0$. Of course, ϕ_0 or $\bar{\phi}_0$ cannot decay and thus is the (single) DM candidate in this theory. We will denote this DM particle and its anti-particle by DM and $\overline{\text{DM}}$, respectively although we do not make this distinction in the text since DM and anti-DM particles are still degenerate.[8]

According to the above-given argument, for Z_3 models, each mother particle can emit either one or two DM particles so that there exist two, three, or four DM particles in the final state (for pair-production of mothers) while there are only two DM particles for Z_2 models. We therefore expect richer structures in the M_{T2} distribution for Z_3 models. Here

- we take as an ansatz only a *single* DM particle in each decay chain for the sole purpose of defining M_T, even if there could be two DM particles in either or both of the two decay chains.

We do so for the following two reasons. Firstly, in the real collider experiment, there is (a *priori*) no clear information on the number of invisible particles involved in the decay process of interest so that each individual decay chain with only one DM is a natural (starting) assumption. Moreover, one can naturally expect (and we will show) that decay events from Z_3 models will show different features in the M_{T2} analysis compared with those for Z_2 models. Therefore, starting with a Z_2 assumption and deriving a "contradiction" in the M_{T2} analysis, we can distinguish Z_3 models from Z_2 ones (which is our primary goal here). In this context, we call such an analysis imposing one-DM-per-chain assumption the "naive" M_{T2} analysis.

For a more systematic consideration let us define the three different events having different number of (a single type of) DM particles as E_2, E_3, and E_4-type, respectively, i.e., each subscript on E simply implies the total number of DM particles in the final state: see Fig. 2, where $\text{SM}_{1,\,2}$ denote the visible/SM final states (irrespective of the actual number of particles in the state) in the decay chains with one and two DM (respectively)[9]. Here the red dashed lines denote any particles charged under dark matter stabilization symmetry (in this section Z_3 symmetry) while the black solid lines/arrows denote any visible/SM particles. One should note that E_4 type events represent the case with 2 DM particles in each decay chain. Also, both decay chains (with one and two DM) might not exist for a *specific* mother so that all three types of events might not occur. Like in Z_2 models, we start with the case with one visible/SM particle in each decay chain, and we consider the case with more than one visible/SM particle in each decay chain in the following subsection. While doing so, we see how the M_{T2} analysis applied to Z_3 models contrasts with Z_2 models.

---

[8]Of course, which of the two particles is denoted anti-DM is a matter of convention. Also, as a corollary, the DM particle should be Dirac fermion or complex scalar in a Z_3 model.

[9]These two SM final states might not or might be identical: we will return to these two possibilities in the next two sections (respectively).
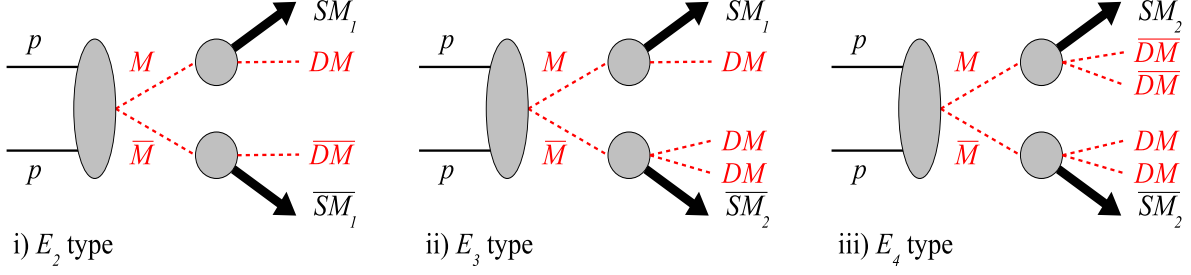
Figure 2: The three types of events in Z_3 models, based on the total number of DM in the event. "M" denotes the mother particle. Each SM final state can have more than one particle, and the subscripts 1 and 2 on SM denote the visible/SM final states in the decay chains with one and two DM, respectively. Note that, based simply on the Z_3 symmetry, if a mother decays into DM, then the *same* mother decays into two *anti*-DM in the other decay chain. Since DM and anti-DM have same mass and are *not* detected, we neglect this distinction between the two henceforth (we already did so thus far). For simplicity, we will also henceforth not differentiate between SM and $\bar{\text{SM}}$ or between M and $\bar{M}$.

3.1 One Visible/SM Particle in Each Decay Chain

In this case the upper edge in the (naive) M_{T2} distribution is determined only by the balanced solution like Z_2 models, and the analytic expressions for the three type events are given as follows (see App. A for details):

$$M_{T2,E_2}^{\max} = M_{T2,E_2}^{\max,bal} = \sqrt{\frac{(M^2 - m_{DM}^2)^2}{4M^2}} + \sqrt{\frac{(M^2 - m_{DM}^2)^2}{4M^2} + \tilde{m}^2} \qquad \text{for } E_2 \ (9)$$

$$M_{T2,E_3}^{\max} = M_{T2,E_3}^{\max,bal} = \sqrt{\frac{(M^2 - m_{DM}^2)(M^2 - 4m_{DM}^2)}{4M^2}} + \sqrt{\frac{(M^2 - m_{DM}^2)(M^2 - 4m_{DM}^2)}{4M^2} + \tilde{m}^2} \quad \text{for } E_3 (10)$$

$$M_{T2,E_4}^{\max} = M_{T2,E_4}^{\max,bal} = \sqrt{\frac{(M^2 - 4m_{DM}^2)^2}{4M^2}} + \sqrt{\frac{(M^2 - 4m_{DM}^2)^2}{4M^2} + \tilde{m}^2} \qquad \text{for } E_4 (11)$$

As a reminder, the events with E_2, E_3 and E_4 represents events with two, three and four dark matter candidates. Note that Eq. (9) has the same form as Eq. (5) in Z_2 models because E_2 type events also contain two DM particles in the final state (just like Z_2 models) whereas the other two types of events do *not* appear in Z_2 models so that the corresponding Eqs. (10) and (11) (and similar ones later) are new/do not appear in previous literature. Substituting $\tilde{m} = m_{DM}$ in Eq. (9) gives the true mother mass M for the value of $M_{T2}^{\max}$ (as expected), but the other two equations give a combination of the true mother and DM masses rather than the true mother mass. Actually, this is not surprising because we have used the naive M_{T2} variable for the $E_{3\,4}$-type events in Z_3 models, whereas the actual physics is different from the physics under which our M_{T2} variable is defined. For example, for E_3 type events there is an asymmetry between the final states of the two decay chains, which is caused by adding one more DM to either of the two decay chains. For E_4 type events, even though the two decay chains have symmetric final states, the "effective" DM
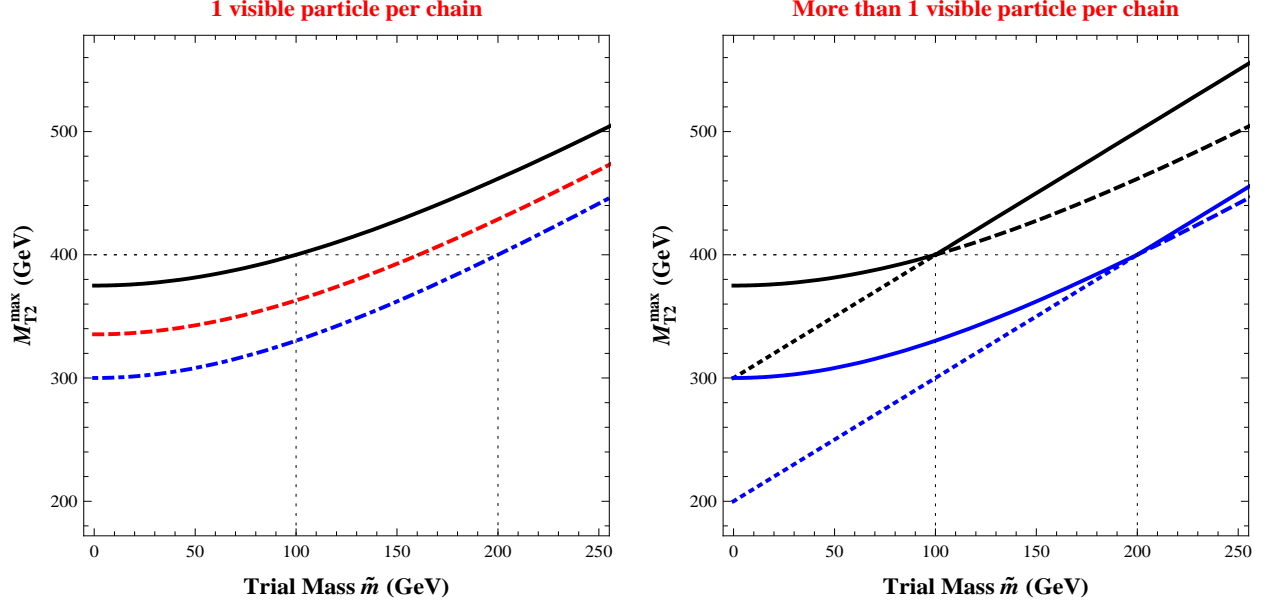
9

Figure 3: Theoretical expectation of $M_{T2}^{\max}$ versus the trial mass $\tilde{m}$ for Z_3 model. The masses of mother and DM particles are 400 GeV and 100 GeV, respectively. The left panel shows the case where there exists only a single visible particle per chain. The black, red, and blue curves are showing the corresponding $M_{T2}^{\max}$ values to E_2, E_3, and E_4 type events over $\tilde{m}$, respectively. The right panel shows the case where there exist more than one visible particle per decay chain. The overall upper edges, $M_{T2}^{\max}$ for E_2 and E_4 type events, are given by the solid black and blue curves, whereas the balanced and unbalanced solutions are denoted by the dashed and dotted curves (respectively) which merge into the solid curves on the right (left)-hand part. The corresponding plot for E_3 type events can be found in the next figure.

mass is twice the true DM mass so that the true mother mass (for the value of $M_{T2}^{\max}$) is in fact obtained by setting $\tilde{m} = 2m_{DM}$ instead as clearly seen from Eq. (11).

All of the theoretical predictions mentioned above are demonstrated in the left panel of Fig. 3. Again, we used 400 GeV and 100 GeV as mother and DM masses. The black solid, the red dashed, and the blue dot-dashed curves represent the theoretical expectations of $M_{T2}^{\max}$ for E_2, E_3, and E_4 type events, respectively (the curve for E_2-type events is of course the same as in right-hand side of Fig. 1). As discussed above, the $M_{T2}^{\max}$ for E_2 type events corresponds to the true mass of the mother particle (here 400 GeV) with the trial DM mass equal to the true DM mass (here 100 GeV) whereas E_4 type events do it for twice the DM mass (here 200 GeV), as shown by the dotted/black lines.

In addition, there are a couple of features to be noted; there is no kink arising in the $M_{T2}^{\max}$ curves for $E_{3,4}$-type events just like the case of a single visible particle per decay chain in Z_2 models (or E_2-type event in Z_3 models). Secondly for any given $\tilde{m}$, the $M_{T2}^{\max}$ values form a hierarchy of

$$M_{T2,E_2}^{\max} > M_{T2,E_3}^{\max} > M_{T2,E_4}^{\max}. \tag{12}$$

10

3.2 More than One Visible/SM Particle in Each Decay Chain

Once more visible particle(s) are added in each decay chain, one could naturally expect that a kink appears like in Z_2 models. The reason is that, just like for Z_2 models, the maximum unbalanced solutions take part in determining the overall upper edge in the M_{T2} distribution together with the balanced solutions. It turns out, however, that this expectation is true only for E_2 and E_4 type events which we discuss to begin with. Again, assuming the intermediate particles are *off*-shell the maximum values of the balanced solutions for E_2 and E_4 type events are simply given (as for the one visible particle case) by Eqs. (9) and (11), respectively, and those of the unbalanced solutions are given as follows:

$$M_{T2,E_2}^{\max,unbal} = M - m_{DM} + \tilde{m} \qquad \text{for } E_2 \qquad (13)$$

$$M_{T2,E_4}^{\max,unbal} = M - 2m_{DM} + \tilde{m} \qquad \text{for } E_4. \qquad (14)$$

Here Eq. (13) is of exactly the same form as Eq. (6) due to the similarity between the decay structures for Z_2 models and E_2 type events while Eq. (14) for E_4-type events is relevant only for Z_3 models, i.e., it is not present in Z_2 models. More quantitatively, the above-given two equations differ by m_{DM} for any given $\tilde{m}$ because one more DM particle is emitted in both decay chains for E_4 type events compared with E_2 type events (see Eqs. (64) and (84) in the App. A).

As mentioned for Z_2 models, the maximum M_{T2} values are given by the larger of the balanced and unbalanced solutions: for E_2 type events as in Eq. (7), and for E_4 type events by:

$$M_{T2,E_4}^{\max} = \max\left[M_{T2,E_4}^{\max,bal}, \ M_{T2,E_4}^{\max,unbal} \right] = \begin{cases} M - 2m_{DM} + \tilde{m} & \text{for } \tilde{m} \geq 2m_{DM} \\ \sqrt{\frac{(M^2-4m_{DM}^2)^2}{4M^2}} + \sqrt{\frac{(M^2-4m_{DM}^2)^2}{4M^2} + \tilde{m}^2} & \text{for } \tilde{m} \leq 2m_{DM}. \end{cases} \qquad (15)$$

Note that there is also a kink for E_4-type events as seen from Eq. (15), but at $\tilde{m} = 2m_{DM}$ (i.e., not m_{DM}), because the effective DM mass for E_4 is given by $2m_{DM}$.

The right panel of Fig. 3 illustrates the above theoretical considerations for E_2 and E_4 type events (of course the curve for E_2-type events is same as right-hand side of Fig. 1). As before, the two straight dotted lines which extend into the right-hand parts of the solid lines indicate the maximum values of the unbalanced solutions while the two dashed curves which extend into left-hand parts of the solid curve indicate the maximum values of the balanced solutions. The actual upper edge in the M_{T2} distribution for any $\tilde{m}$ is given by the black (for E_2 type events) or blue (for E_4 type events) solid curves. Identifying the location of the kink in E_2-type events and its corresponding $M_{T2}^{\max}$ enables us to determine the masses of mother and DM particles separately (just like in Z_2 models). The figure also shows the kink for E_4-type events, but located at $\tilde{m} = 200$ GeV (i.e., $2m_{DM}$, as expected) and $M_{T2}^{\max} = 400$ GeV. This observation can be used as a cross-check for the determination of M and m_{DM} based on E_2-type events (again, this feature is new in Z_3 models relative to Z_2).
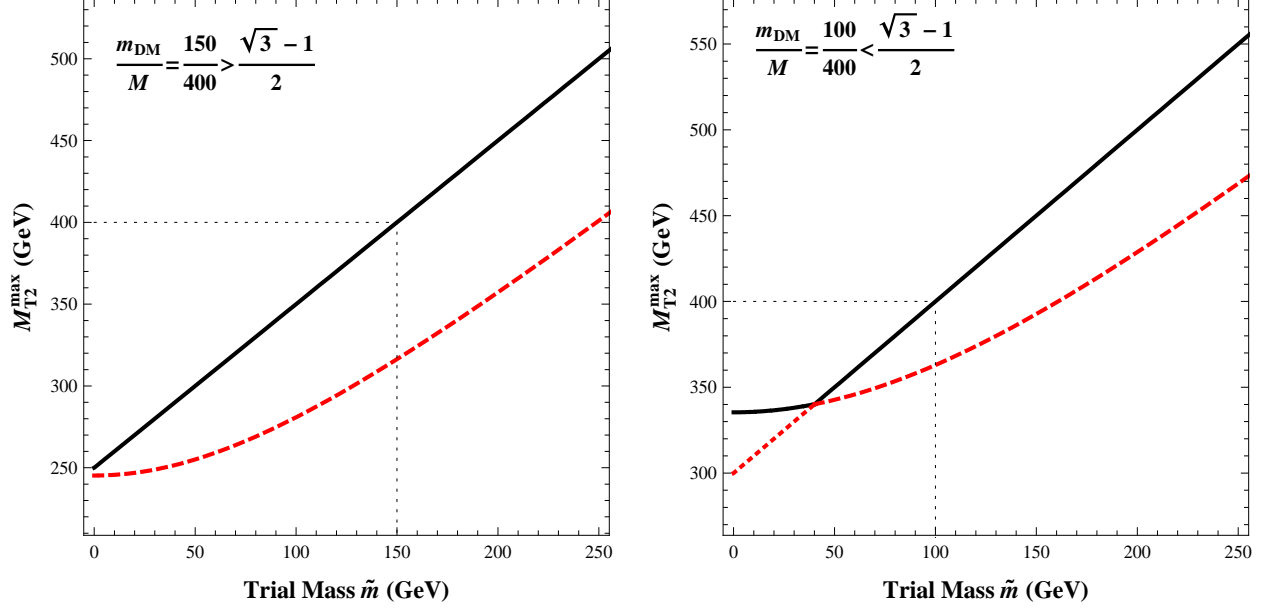
11

Figure 4: Theoretical expectation of $M_{T2}^{\max}$ versus the trial mass $\tilde{m}$ for E_3 type events. The mass of mother particle is 400 GeV for both cases, but the masses of DM particle to be used are 150 GeV and 100 GeV for the left panel and the right panel, respectively. For both cases, the black solid lines give the maximum of M_{T2}, whereas the dashed curves give the maximum for the balanced solution. The maximum for the unbalanced solution coincides with the solid line on the left panel, whereas on the right panel, it is given by the dotted straight line (which extends into the right-hand part of the solid line).

On the other hand, as far as E_3 type events (which are absent in Z_2 models)) are concerned, whether or not there exists a kink depends on the mass hierarchy between mother and DM particles (see App. B for details). Again, assuming *off*-shell intermediate particles the maximum balanced solution is simply given by Eq. (10) (just like the case of one visible particle per decay chain), whereas the maximum unbalanced solution has the same form as that for E_2 type events because one of the two decay chains still emits a single DM particle in the final state (see Eqs. (64) and (84) in the App. A).

$$M_{T2,E_3}^{\max,unbal} = M - m_{DM} + \tilde{m} \qquad \text{for } E_3 \qquad (16)$$

If the ratio of the DM mass to the mother mass is larger than $(\sqrt{3}-1)/2$, it turns out that the maximum unbalanced solution given in Eq. (16) is always bigger than the maximum balanced solution given in Eq. (10) so that

$$M_{T2,E_3}^{\max} = \max\left[M_{T2,E_3}^{\max,bal}, \ M_{T2,E_3}^{\max,unbal} \right] = M - m_{DM} + \tilde{m} \qquad \text{for } \frac{m_{DM}}{M} \geq \frac{\sqrt{3}-1}{2} \text{ and for all } \tilde{m}. \quad (17)$$

The left panel of Fig. 4 clearly confirms our expectation (based on above equation) that there occurs no kink in the upper edge of M_{T2} as a function of the trial DM mass, i.e., the upper edge

in the M_{T2} distribution is always determined by the unbalanced solution (black solid line), not by the balanced solution (red dashed curve). Here we adopted $M = 400$ GeV and $m_{DM} = 150$ GeV, and thus the ratio between them is obviously larger than $(\sqrt{3}-1)/2$.

On the other hand, once the ratio of DM to mother mass is smaller than $(\sqrt{3}-1)/2$, the competition between the balanced and the unbalanced solutions results in

$$
M^{\max}_{T2,E_3} = \max\left[M^{\max,bal}_{T2,E_3}, M^{\max,unbal}_{T2,E_3}\right]
$$

$$
= \begin{cases} M - m_{DM} + \tilde{m} & \text{for } \tilde{m} \geq m' \\[2ex] \sqrt{\frac{(M^2-m^2_{DM})(M^2-4m^2_{DM})}{4M^2}} + \sqrt{\frac{(M^2-m^2_{DM})(M^2-4m^2_{DM})}{4M^2} + \tilde{m}^2} & \text{for } \tilde{m} \leq m' \end{cases}
$$

$$
\text{and for } \frac{m_{DM}}{M} \leq \frac{\sqrt{3}-1}{2} \tag{18}
$$

where

$$
m' = \frac{(M-m_{DM})\left(\sqrt{(M^2-m^2_{DM})(M^2-4m^2_{DM})} - M(M-m_{DM})\right)}{2M(M-m_{DM}) - \sqrt{(M^2-m^2_{DM})(M^2-4m^2_{DM})}}. \tag{19}
$$

We see that there is a kink at $\tilde{m} = m'$. Here m' is *not* simply the true DM mass but it is given by a combination of the true mother and DM masses (in fact, it is smaller than the true DM mass), which is clearly different from that in Z_2 models. The functional behavior of $M^{\max}_{T2}$ for this case is shown in the right panel of Fig. 4. Here we took $m_{DM} = 100$ GeV which makes the ratio smaller than $(\sqrt{3}-1)/2$. As before, the maximum M_{T2} for the balanced and unbalanced solutions are shown by the dashed and dotted curves (which extend into the black solid curve to the RHS and LHS). The final maximum M_{T2} is given by the larger of these two solutions (black solid curve) which clearly shows a kink at a value of $\tilde{m}$ which is different from the actual DM mass $m_{DM} = 100$ GeV (shown by the vertical black dotted line) as expected based on above discussion. Of course, we can still evaluate the masses of mother and DM particles (using E_3-type events only) by obtaining $M^{\max}_{T2}$ and m' from the above M_{T2} analysis, substituting them into Eqs. (18) and (19), and solving those two equations about M and m_{DM}.

Next, let us investigate the hierarchy among the three $M^{\max}_{T2}$ values for E_2, E_3, and E_4 type events. Although a bit more complicated than the one visible particle case, it is nonetheless straightforward to derive this hierarchy based on above equations, We have a following hierarchy among the $M^{\max}_{T2}$ values for the three types (cf. the one visible particle case shown in Eq. (12)):

$$
M^{\max}_{T2,E_2} = M^{\max}_{T2,E_3} > M^{\max}_{T2,E_4} \qquad \text{for } \tilde{m} \geq m_{DM}
$$

$$
M^{\max}_{T2,E_2} > M^{\max}_{T2,E_3} > M^{\max}_{T2,E_4} \qquad \text{for } \tilde{m} \leq m_{DM}. \tag{20}
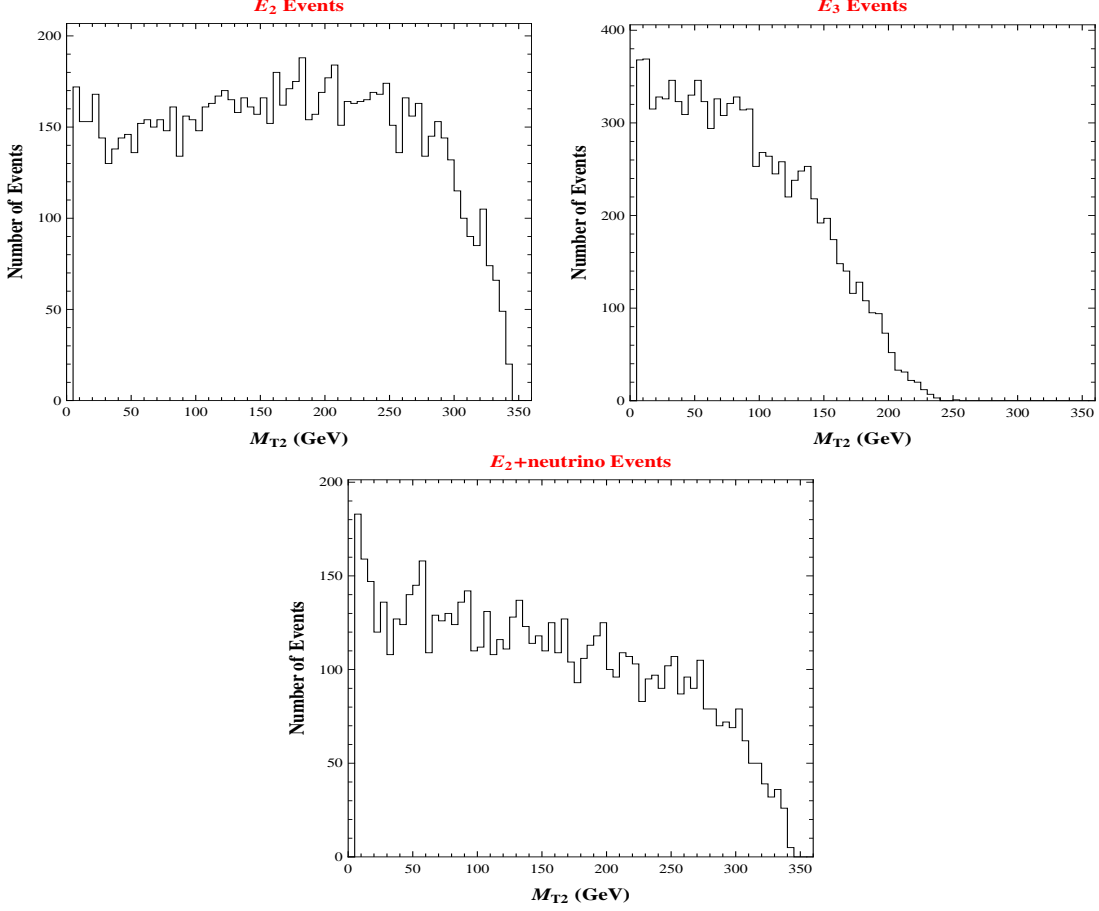$$

Figure 5: The M_{T2} distributions for E_2 (top left) and E_3 (top right) type events and $E_2 + \nu$ events (bottom). The mother and the DM particle masses are 400 GeV and 150 GeV, respectively, and the trial DM mass ($\tilde{m}$) used is 6 GeV.

3.3   Shapes of M_{T2} Distributions

Before closing the present section, let us examine the shape of the M_{T2} distributions for Z_3 cases. For this purpose we simulated events using MadGraph/MadEvent [38]. Here and in sections 5.1.1 and 5.1.2, we make the following assumptions (mostly for simplicity): (a) effects of spin correlations are neglected in both production and decay of mother particles, i.e., we assumed scalar particles only in our simulations,; (b) the beam is proton-proton with 14 TeV total energy in the center of mass frame (motivated by the LHC parameters); (c) the non-colored (scalar) mother particles are pair-produced via s-channel exchange (of another scalar particle) and finally (d) only the *relative* values of the number of events (on vertical scale) are meaningful, i.e. only the *shape* of the distributions is the robust aspect of our analysis.

For all the simulations in *this* section, the masses of mother and DM particles used in the (toy) model are 400 GeV and 150 GeV, respectively, we took a *single* visible particle per decay chain

for simplicity and chose a small trial DM mass $\tilde{m}$ (here 6 GeV) for the purpose of illustration. The upper left panel of Fig. 5 demonstrates the M_{T2} distribution for E_2 type events. Obviously, this is similar to the M_{T2} distribution for events in Z_2 models [2, 3, 4], which is not surprising because E_2 type events also has only two dark matter particles in the final state like Z_2. The (naive) M_{T2} distribution for E_3 type events illustrated in the upper right panel of Fig. 5 has two notable features. As expected from the analytic expressions given before, first of all, the location of the upper edge is clearly lower than that for E_2 type events (or for Z_2 models). Secondly, the shape of M_{T2} distribution for E_3 type events shows a long tail near the upper edge compared with E_2 type events (which have relatively sharp upper edge): this is because more physical constraints (e.g., rapidity) between decay products should be satisfied in E_3 type events in order that they form a kinematic configuration to give maximum M_{T2}, thereby reducing the corresponding number of events near $M_{T2}^{\max}$.

This feature of a (relatively) long tail is also true for a special case in Z_2 models with three invisible particles in the full event one of which is a (massless) SM neutrino, i.e., with one DM in one decay chain, but one DM and a neutrino in the other (henceforth we call it $E_2 + \nu$ events)[10]. The bottom panel of Fig. 5 demonstrates the M_{T2} distribution for $E_2 + \nu$ events, assuming intermediate particles are off-shell [11]. At the upper edge it shows a tail which is longer than that for E_2 type events (or neutrino-less events in Z_2 models), but which is not as long as that for E_3 type events[12]. Such a shape is not surprising because the additional invisible particle (neutrino) in $E_2 + \nu$ vs. E_2-type events is massless so that $E_2 + \nu$ events can be understood as a transitional type between E_2 and E_3 type events. However, it is crucial to note that the location of the upper edge for the $E_2 + \nu$ events is the *same* as that for usual (i.e., neutrino-less) events in Z_2 models with only a single massive invisible particle per decay chain, because the effective DM mass in former decay chains is also m_{DM}. We can therefore distinguish the $E_2 + \nu$ events from the E_3-type events in Z_3 models by observing the location of the upper edge: the latter events will have a smaller edge.

4   Applications: Non-Identical Visible Particles in the Two Decay Chains

Next, we apply the theoretical observations on the M_{T2} technique for Z_2 and Z_3 models, which are described in the previous sections, for distinguishing Z_3 models from Z_2 ones in some *specific* cases. Like in the previous sections, we assume (for simplicity) pair-produced (same) mother particles and that all visible particles are massless and use the naive M_{T2} analysis for all events. As mentioned earlier, in Z_3 models each mother particle can decay into either one or two dark matter particles

---

[10] M_{T2} distributions for such events have been studied in [3] and in [24].

[11] As for the events with three (or more) DM, we assume here that there is a single (massive) invisible particle in each decay chain for the purpose of defining M_T.

[12] This feature of a long tail in $E_2 + \nu$-type events is valid even for the case of more than one visible particles in each decay chain.

along with visible/SM particle(s). Here,

- we consider a mother particle in a Z_3 model for which *both* these decay chains (with one and two DM, respectively) exist.

Similarly, in Z_2 models the mother particles can only decay into a single dark matter particle along with visible/SM particle(s). Here, we assume two such decay chains for a Z_2-mother which have the same visible final states as the above two Z_3-mother decay chains (respectively). The idea behind this choice is that such a Z_2 model could easily fake Z_3 one (at least based on the identity of the visible states). This motivates us to distinguish these two types of DM stabilization symmetry using the M_{T2} variable.

For later convenience, we divide the discussion into two cases based on whether or not the visible state in the decay chain with one DM is identical to the one in the decay chain with two DM in the Z_3 model. We begin with the case where the SM final states in the two decay chains are not identical (this includes the case of partial overlap between these final states). Following the notation of previous section, let us denote $SM_{1,\,2}$ to be these SM final state particles – whether they consist of one or more SM particles – in the two decay chains. And, for the Z_3 model, assume that SM_1 comes with one DM particle and SM_2 is associated with two DM particles.[13] We thus have three *distinct* (based simply on identity of visible states) types of events in both the Z_3 and Z_2 models, denoted by SM_{11}, i.e., SM_1 on each side/from each mother and similarly $SM_{12,\,22}$. Clearly, for Z_3 models, these three types of events correspond (respectively) to $E_{2,3,4}$-type events mentioned in the previous section and shown in Fig. 2 (with $SM_1 \neq SM_2$). Hence, we can apply the formulae for the theoretical predictions of $M_{T2}^{\max}$ for E_2, E_3, and E_4 type events derived in the previous section to the $SM_{11,\,12,\,22}$ events.

4.1 One Visible/SM Particle in Each Decay Chain

As a further subcase, we assume that $SM_{1,2}$ consist of only one particle. Clearly, the upper edges of the M_{T2} variable for SM_{11}, SM_{12}, and SM_{22} are given by Eqs. (9), (10), and (11), respectively. As is obviously seen from the left panel of Fig. 3 or equivalently Eq. (12), the location of the upper edge for SM_{12} or SM_{22} is lower (for *all* trial DM mass $\tilde{m}$: cf. the case of more than one visible particles below) than that for SM_{11} (for the same mother and DM masses). In contrast, in Z_2 model we have the same expression for $M_{T2}^{\max}$ given by Eq. (5) for *all* of SM_{11}, SM_{12}, and SM_{22} because they all involve two DM particles in the final state. Thus,

- different edges for the $SM_{11,\,12,\,22}$ events (in particular, larger for SM_{11}) can be evidence for Z_3 models, i.e., they provide discrimination between Z_2 and Z_3 models[14].

---

[13]Since a Z_2 model does not allow 2 DM particles in each decay chain, SM_1 and SM_2 are both emitted with only 1 DM in the final state in this model.

[14]unless multiple mother particles in the Z_2 models decay into the identical final state.

We can be further quantitative:

- for Z_3 models we can measure the masses of mother and DM separately as follows (in spite of absence of kink in left panel of Fig. 3).

Note that the theoretical formulae for $M_{T2}^{\max}$ in Eq. (9) through Eq. (11) – considered as a function of trial mass $\tilde{m}$ – have a structure of $\sqrt{C} + \sqrt{C + \tilde{m}^2}$ where C is a constant. So, the idea is to choose an arbitrary trial mass, then calculate the corresponding $M_{T2}^{\max}$ from the *experimental* data and thus determine the above-defined C. Also, in our specific case where visible particles are assumed massless, the *theoretical* formula for each C is written only in terms of the mother mass and the DM mass:

$$\frac{(M^2 - m_{DM}^2)^2}{4M^2} = \frac{\left((M_{T2,E_2}^{\max})^2 - \tilde{m}^2\right)^2}{4(M_{T2,E_2}^{\max})^2} \equiv C_{E2} \tag{21}$$

$$\frac{(M^2 - m_{DM}^2)(M^2 - 4m_{DM}^2)}{4M^2} = \frac{\left((M_{T2,E_3}^{\max})^2 - \tilde{m}^2\right)^2}{4(M_{T2,E_3}^{\max})^2} \equiv C_{E3} \tag{22}$$

Solving the above-given two equations, we obtain *both* mother and DM masses [15]:

$$M = \frac{2}{3\sqrt{C_{E2}}}(4C_{E2} - C_{E3}) \tag{23}$$

$$m_{DM} = \frac{2}{3\sqrt{C_{E2}}}\sqrt{(4C_{E2} - C_{E3})(C_{E2} - C_{E3})} \tag{24}$$

This situation is somewhat like the double edge signal for single mother decay studied in reference [36], where it was again possible to obtain mother and DM masses from the two edges in invariant mass distribution of visible/SM final state.

On the other hand, for Z_2 models, we obtain only a *combination* of mother and DM masses from the (single) measurement of $M_{T2}^{\max}$, given by

$$\frac{(M^2 - m_{DM}^2)^2}{4M^2} = \frac{\left((M_{T2}^{\max})^2 - \tilde{m}^2\right)^2}{4(M_{T2}^{\max})^2} \equiv C, \tag{25}$$

and thus it is *not* possible to determine mother and DM masses separately.

4.2   More than One Visible/SM Particle in Each Decay Chain

In this case, there is more interesting behavior of $M_{T2}^{\max}$ than the case of one visible particle per chain [16]. The upper edges of M_{T2} for $\mathrm{SM}_{11,\,12,\,22}$ events are now obviously given by Eqs. (7), (17),

---

[15]The upper edge from SM_{22} provides redundant information, but of course can be a cross-check.

[16]In the SM_{12} events, the endpoints of the *visible* invariant mass distributions for the two sides of the event/decay chains will be different in Z_3 models, i.e., in E_3-type events (vs. being the same in Z_2 models), already providing a discrimination between the two types of models [36]. However, developing another technique for distinguishing Z_3 from Z_2 models based on M_{T2} can still be useful.

(18) and (15), respectively. As discussed in Eq. (20), the upper edge for SM_{12} is the *same* as that for SM_{11} (cf. one visible particle case above) for $\tilde{m} > m_{DM}$, but is lower for $\tilde{m} < m_{DM}$ than that for SM_{11}. And, the upper edge for SM_{22} events always lower than SM_{11}. This fact enables us to *distinguish* Z_3 models from Z_2 ones because in Z_2 models the upper edges for $SM_{11,\,12,\,22}$ coincide for *all* $\tilde{m}$ (just like the case with one visible particle in each decay chain).

Moreover, there occurs a kink in the upper edge of M_{T2} as a function of the trial DM mass as discussed in the previous sections. Due to the existence of this kink structure, SM_{11} itself is sufficient for the purpose of determining mother and DM masses (again, unlike one visible case): the trial mass which gives rise to a kink is the true DM mass and its corresponding $M_{T2}^{\max}$ is the true mother mass. (Of course this is how one can measure the masses of mother and DM particles separately even in Z_2 models.) Such a direct measurement of mother and DM masses leads us to

- a *prediction* (cf. one visible case) on the location of the upper edges for the *other* two types of events, namely SM_{12} and SM_{22}, a confirmation of which can provide evidence for Z_3 symmetry as underlying physics[17].

For SM_{12}, i.e., E_3-type events, actually, there are more interesting aspects of the kink structure in $M_{T2}^{\max}$ due to the dependence on the ratio of DM and mother masses: as discussed in Sec. 3, the critical ratio is given by

$$\frac{m_{DM}}{M} = \frac{\sqrt{3}-1}{2}. \tag{26}$$

The kink is present only when the ratio of DM and mother masses is less than the above-given critical ratio. In this case, the kink location can be predicted by substituting mother and DM masses measured from the kink in SM_{11} into Eq. (19) so that it can provide a *further* verification for Z_3 symmetry[18].

Finally, note that another way to distinguish Z_3 from Z_2 models in this case was discussed in [36]. The idea is to use SM_{12}, i.e., E_3-type, events in Z_3 models, where edges in invariant mass distributions of *visible* particles on each side are different, i.e., $(M - m_{DM})$ and $(M - 2\,m_{DM})$ (vs. the two edges being the same for Z_2 models).

4.3   Signal Fakes by an (Effective) 2nd DM Particle

In the two previous sections we have focused on decay processes with a single type of DM particle in the final state (for both Z_3 and Z_2 models). The crucial observation for the sake of discriminating Z_3 from Z_2 models is that Z_3 models have more event-topologies (i.e., E_2, E_3, and E_4 type events with different upper edges in M_{T2} distributions) than the case of Z_2 (which has a single upper edge),

---

[17]We can also predict (and then verify) location of kink in SM_{22} events. Alternatively, we can use kink in SM_{22}, i.e., E_4-type events to determine the mother and DM masses and then make predictions.

[18]Alternatively, this kink can be used to determine mother and DM masses, which are then used to predict edges/kinks in other events.

regardless of the number of visible/SM particles in each decay chain. In turn, this contrasting feature is due to the different possibilities in *each* decay chain in Z_3 models, i.e., presence of one or two DM (unlike only one DM in Z_2 case).

However, Z_2 models can also acquire such different possibilities for decay chains (and thus fake Z_3 signals in the M_{T2} analysis) if we assume that there is a *second* DM (obviously Z_2-odd) particle (with larger mass) denoted by DM$'$ into which the Z_2-mother can decay, i.e., there are actually two (absolutely) stable DM particles in a Z_2 model [40]. Clearly, even with only one DM in a Z_2 model, a similar effect can arise from a mother decaying into an (Z_2-odd) *on*-shell color/electrically neutral particle which *decays* (into DM particle and SM, possibly visible), but outside the detector (i.e., there exists a Z_2-odd particle – other than the DM – which is stable and invisible as far as detector is concerned). Another related possibility is that there is a Z_2-odd (on-shell) neutral particle which decays *in*side the detector, but invisibly, i.e., into DM and invisible SM, for example, neutrino. A classic example of the last type is found in supersymmetry where sneutrino decaying into neutrino and lightest neutralino (which is assumed to be the lightest supersymmetric particle, i.e., DM). Even in the latter two cases, there is "effectively" (i.e., as far as the collider analysis is concerned) a second "DM" and so we will denote it also by DM$'$. In particular, in the last case mentioned above, i.e., even if there is an (on-shell) neutral particle decaying invisibly inside detector, the theoretical prediction of M_{T2} variable is same as with a DM$'$ of same mass as this neutral mother particle.

Here, we note that the reference [10] has studied such (asymmetric) events using an M_{T2} type analysis, in particular, variants of the usual M_{T2} variable have been developed. As before, we will instead apply the naive/usual M_{T2} variable, i.e., assume (again, just for the purpose of constructing M_{T2}) that there is a single and same DM in both decay chains.

In more detail, the above case in Z_2 models give rise to "Z_3-faking" signals is as follows. As before, consider pair production of single mother such that decay chains with DM and DM$'$ are both allowed. Consequently, we obtain three distinct decay topologies for the full event: two DM, one DM and one DM$'$ and two DM$'$. We will denote these three types of events by E_2', E_3', and E_4' since they obviously resemble (and thus can fake) E_2, E_3, and E_4 type events being found in Z_3 models, respectively. In particular, we can expect three different upper edges for M_{T2} in E_2', E_3', and E_4'-type events[19]. Explicitly, the maximum balanced M_{T2} solutions for them (for both the cases with one visible particle per decay chain and more than one visible particle per decay chain)

---

[19]An extreme case is when DM$'$ is massless, for example, SM neutrino. However, in this case, as mentioned in section 3.3, the upper edges for E_3' (denoted by $E_2 + \nu$ event in section 3.3) and E_4'-type events will be *same* as for E_2'-type events. Thus this case can be easily distinguished from Z_3 models.

are simply given as follows:

$$M_{T2,E_2'}^{\max,bal} = \sqrt{\frac{(M^2 - m_{DM}^2)^2}{4M^2}} + \sqrt{\frac{(M^2 - m_{DM}^2)^2}{4M^2} + \tilde{m}^2} \qquad \text{for } E_2' \quad (27)$$

$$M_{T2,E_3'}^{\max,bal} = \sqrt{\frac{(M^2 - m_{DM}^2)(M^2 - m_{DM}'^2)}{4M^2}} + \sqrt{\frac{(M^2 - m_{DM}^2)(M^2 - m_{DM}'^2)}{4M^2} + \tilde{m}^2} \quad \text{for } E_3' \quad (28)$$

$$M_{T2,E_4'}^{\max,bal} = \sqrt{\frac{(M^2 - m_{DM}'^2)^2}{4M^2}} + \sqrt{\frac{(M^2 - m_{DM}'^2)^2}{4M^2} + \tilde{m}^2} \qquad \text{for } E_4', \quad (29)$$

and the maximum unbalanced M_{T2} solutions (only for the case with more than one visible particle per decay chain) are given as follows:

$$M_{T2,E_2'}^{\max,unbal} = M - m_{DM} + \tilde{m} \qquad \text{for } E_2' \qquad (30)$$

$$M_{T2,E_3'}^{\max,unbal} = M - m_{DM} + \tilde{m} \qquad \text{for } E_3' \qquad (31)$$

$$M_{T2,E_4'}^{\max,unbal} = M - m_{DM}' + \tilde{m} \qquad \text{for } E_{4'}. \qquad (32)$$

Here $m_{DM}'(> m_{DM})$ denotes the mass of the second DM-like particle. Again, all three types actually contains *two* DM/DM-like particles, i.e., the subscripts on E' do not imply the number of DM particles in a full decay chain but rather indicate the respective topologies in Z_3 models which they fake. Note that if we set $m_{DM}' = 2m_{DM}$, then the above edges are exctly the ones in a Z_3 model (see Eqs. (9) through (11) and Eqs. (13), (14), and (16) from previous sections. This feature is as expected since for $E_{3,4}$-type events (in Z_3 models) which are at the edge of the respective M_{T2} distributions, the two DM from *same* mother are collinear so that their invariant mass is $2m_{DM}$, i.e., the decay chain with two DM effectively has *single* DM of this mass as far as M_{T2}-edge is concerned.

Despite the fact that such Z_2 events with second DM-like particle can introduce three decay topologies, we can still differentiate Z_3 and Z_2 models. However, the strategies to be applied depend on the number/identity of visible particles in each decay chain. In this section, we consider the case where the visible particles in decay chain with DM (denote by SM_1, following the notation used earlier) is different than the visible particles (denoted by SM_2) that in decay chain with DM' in Z_2 model or two DM (in Z_3 model). Thus, the three types of events SM_{11}, SM_{12} and SM_{22}, i.e., distinguishable from the identity of SM visible particles, have different edges since they correspond to the E_2', E_3', and E_4'-type events in a Z_2 model or (as mentioned in previous section) E_2, E_3, and E_4-type events in a Z_3 model. This case can be further sub-divided into one and more than one visible particles in each decay chain.

In the case with one visible particle per decay chain, one may distinguish Z_2 and Z_3 models by examining the *shape* of the above three M_{T2} distributions. The idea is that, as explicitly mentioned above, E_2', E_3', and E_4' all have only *two* DM/DM-like particles, i.e., two DM, one DM and one DM', and two DM', and therefore, they have a similar shape of the M_{T2} distribution as the E_2-type

event. The implication of this observation is E_2', E_3', and E_4' all give a sharp upper edge in the M_{T2} distribution. On the other hand, in the decay chain with two DM in $E_{3,4}$-type events of Z_3 models, in general (i.e., away from edge of M_{T2}), the two DM are not collinear so that their invariant mass of two DM is not $2m_{DM}$, in fact, this invariant mass is not even fixed. Thus, even if the above three M_{T2}-*edges* for Z_3 models are identical to those for Z_2 models with two different DM (with the second one being twice as heavy as first one), the shapes are not expected to be similar. In fact, E_3 and E_4 type events in Z_3 models give a (relatively) longer tail as already discussed in Sec. 3.3. Hence, if one of the M_{T2} distributions for $SM_{11,\,12,\,22}$ events – again, corresponding to the three different topologies – has a sharp upper edge and two of which have a longer tail, then it is likely that such events originate from Z_3 models.

On the other hand, once there exist more than one visible particle in each decay chain, the shape is no longer a useful discriminator. The reason is that, in general, clear sharp edges in the M_{T2} distributions are not expected here (unlike the cases with one visible particle per decay chain), i.e., the number of events/statistics at the M_{T2}-upper edge is small in this case: in turn, this feature is due to more constraints which need be satisfied (see Sec. 3). Instead, we can take the advantage of "kink" in the plot of $M_{T2}^{\max}$ versus the trial DM mass, which allows us to determine the masses of mother and DM particles separately. Using the SM_{11} events, one can evaluate M and m_{DM} as mentioned in the previous section, *assuming* that it is a Z_3 model. Then we predict the locations of upper edge and the locations of kink for the $SM_{12,\,22}$ events. If the underlying physics is a Z_2 model (with two different DM particles) instead, then these predictions do not match with the experimental results from the associated M_{T2} analysis. This is because, in general, the mass of the second DM-like particle, m_{DM}' is not equal to twice of DM mass, $2m_{DM}$. In other words, the cross-checking of mother and DM masses between SM_{11} and $SM_{12,\,22}$ events enables us to separate Z_3 models from Z_2.

5 Identical Visible Particle(s) in the Two Decay Chains

Next, we consider the case of the visible particle(s) in the two decay chains with one and two DM (for Z_3 models) being the same. In this case, in the Z_3 models, we can not separate $E_{2,3,4}$ type events using simply the identities of the visible particles, i.e., $SM_1 = SM_2$ in Fig. 2 (unlike in the previous section). Obviously, we add the three (i.e., E_2, E_3, and E_4-type) distributions of M_{T2}, whose behaviors were discussed above (for non-identical case), to obtain the observable M_{T2} distribution in Z_3 models. Of course, for Z_2 models (which could potentially fake the Z_3 models), there are then only E_2-type and possibly $E_2 + \nu$ events that we discussed earlier.

If we have only one visible particle in each decay chain, the M_{T2} distribution for the E_3 type events *always* (i.e., for all $\tilde{m}$, cf. more than one visible case discussed below) has a lower $M_{T2}^{\max}$ than for the E_2 type events (see the left panel of Fig. 3), so that in principle their addition/combination

would give rise to a "kink" in the M_{T2} distribution[20] (again for Z_3 model, but not for Z_2 model).[21] It turns out, however, that the visibility of this kink is not clear because the M_{T2} distribution for E_3 type events has a longer tail (that for E_2-type events) as discussed in Sec. 3 (see the right panel of Fig. 5). It also turns out that the kink will get further smeared out once uncertainties in measurements are taken into account. In other words, this kink is not evidence for Z_3 models since it could be faked by statistical fluctuations in the distribution or experimental errors.

On the other hand, if there exists more than one visible particle in each decay chain, the M_{T2} distribution for Z_3 model shows somewhat different behavior. As discussed in detail in Sec. 4.2, for trial DM mass above the true DM mass, the upper edge of M_{T2} distribution for E_2 and E_3 type events are the same. However, the upper edge of M_{T2} distribution for E_3 type events is *increasingly* lower than that for E_2 type for trial DM mass below the true DM mass[22]. We therefore expect a "moving" kink (as we vary $\tilde{m}$) in the M_{T2} distribution – such a kink starts to appear for trial mass below the true DM mass (i.e., no kink would appear in the total M_{T2} distribution for larger trial masses) and the gap between the kink position (i.e., corresponding to the E_3 edge) and the overall upper (i.e., E_2) edge is increasing as the trial mass becomes smaller[23]. This "moving" feature of the kink in the total M_{T2} distribution can be a further (i.e., beyond simply *existence* of kink) evidence for the existence of E_3 type events and thus a proof of Z_3 models. However, even though the kink is "moving", it is still hard to identify it in the M_{T2} distribution, and thus we do not rely on these kinks as a way to distinguish between Z_2 and Z_3 models.

These observations motivate us to introduce new methods to separate E_3 type events from E_2 type events.[24] In the following (two) subsections, we develop such a method, and then we apply them to the two specific cases (i.e., one visible particle and more than one visible particles in each decay chain), and see how to use them to distinguish between Z_2 and Z_3 models.

5.1 Separating E_2 and E_3 Type Events using P_t/H_t Ratio

To separate E_2 and E_3 types of events, we can utilize the fact that E_2 type events have one DM per decay chain, and E_3 type events have one DM in one decay chain and two DMs in the other decay chain. In other words, for E_3 type events, the visible particle(s) in the decay chain having two DMs in the final state carry less momentum/energy (than in the other decay chain). Thus the ratio between the momentum/energy of visible particle(s) on the two decay chains are expected to be (relatively) sizeable on average (compared to E_2 type events). In order to find out how this

---

[20]Such a kink in the M_{T2} *distribution* is not to be confused with that in the plot of $M_{T2}^{\max}$ as a function of $\tilde{m}$.

[21]Adding events of E_4 type, i.e., two DMs in each decay chain, will introduce another, but even less visible, kink.

[22]To be more precise, the gap between the two edges *relative* to mother/DM masses increases.

[23]In the one visible particle case, the gap between the edges in $E_{2,\,3}$-type events, again relative to mother/DM masses, is roughly constant with trial mass so that kink in M_{T2} distribution does not move.

[24]Once we separate these two types, we can repeat the program described in detail in Sec. 4, i.e., either determine the masses of mother and DM particles from the the upper edges of M_{T2} in these two types of events for the case of one visible particle in each decay chain or *predict* the upper edge for E_3-type events (using measurements in E_2-type events) for the more than one visible particle case.

$R_{P_t}^{\min}$	2	3	4	5	6	7	8	9	10
E_2	0.3375	0.1629	0.0957	0.0612	0.0413	0.0285	0.0225	0.0178	0.0144
E_3	0.7929	0.6105	0.4649	0.3696	0.303	0.2525	0.21	0.1774	0.1522
E_2 + neutrino	0.5366	0.3323	0.2319	0.1733	0.1342	0.1101	0.0887	0.0738	0.0628

Table 1: The percentage of surviving events in E_2, E_3 and $E_2 + \nu$ events for different choice of $R_{P_t}^{\min}$ for the case with one visible particle per decay chain. The mother mass is M = 400 GeV and the DM mass is m_{DM} = 150 GeV.

intuition plays out in real situations, we begin with the case where there exists only a single visible particle per decay chain, and then move on to the case where there exist more than one visible particles per decay chain.

5.1.1 One Visible/SM Particle in each Decay Chain

For the case with one visible particle per decay chain, we consider the P_t ratio of the two visible particles as follows:

$$R_{P_t} = \frac{P_t^{\max}}{P_t^{\min}}, \tag{33}$$

where $P_t^{\max}$ is the larger P_t of the two visibles coming from two separate decay chains, and $P_t^{\min}$ is the smaller one. From our physical intuition mentioned above, we expect the R_{P_t} for E_3 type events to be larger (on average) than that for E_2 type events[25]. To verify this expectation, we did a simulation using MadGraph/MadEvent for a (toy) model with mother mass M = 400 GeV and DM mass m_{DM} = 150 GeV. The R_{P_t} distributions for E_2 and E_3 type events are shown in Fig. 6. We can see clearly that R_{P_t} for E_3 type events is generally larger than that for E_2 type events. For comparison, we also included the R_{P_t} distribution for $E_2 + \nu$ events (i.e., two DM particles and an extra invisible, but massless, particle in the full event) in Fig. 6. One can easily see that the $E_2 + \nu$ events have on *average* larger R_{P_t} than that for pure E_2 type events, but smaller R_{P_t} than that for E_3 type events. This observation agrees with our expectation: in the $E_2 + \nu$ events, we have only one extra *massless* invisible particle (relative to E_2-type events), while in E_3 type events, we have one extra *massive* invisible particle so that the disparity between the visible particle momenta on the two sides in the former case should be relatively smaller.

Due to different R_{P_t} distributions of E_2 and E_3 type events, we can try to distinguish them by doing a cut $R_{P_t} > R_{P_t}^{\min}$. The percentage of "surviving" events in E_2 and E_3 type events according to different choice of $R_{P_t}^{\min}$ are shown in Table 1. For comparison, we also include $E_2 + \nu$ events in Table 1. We can see that the survival rates for E_2 type events are fairly independent of mother and DM masses, since in this type of events the energies of the visible particles in two decay chains are always comparable. Therefore,

---

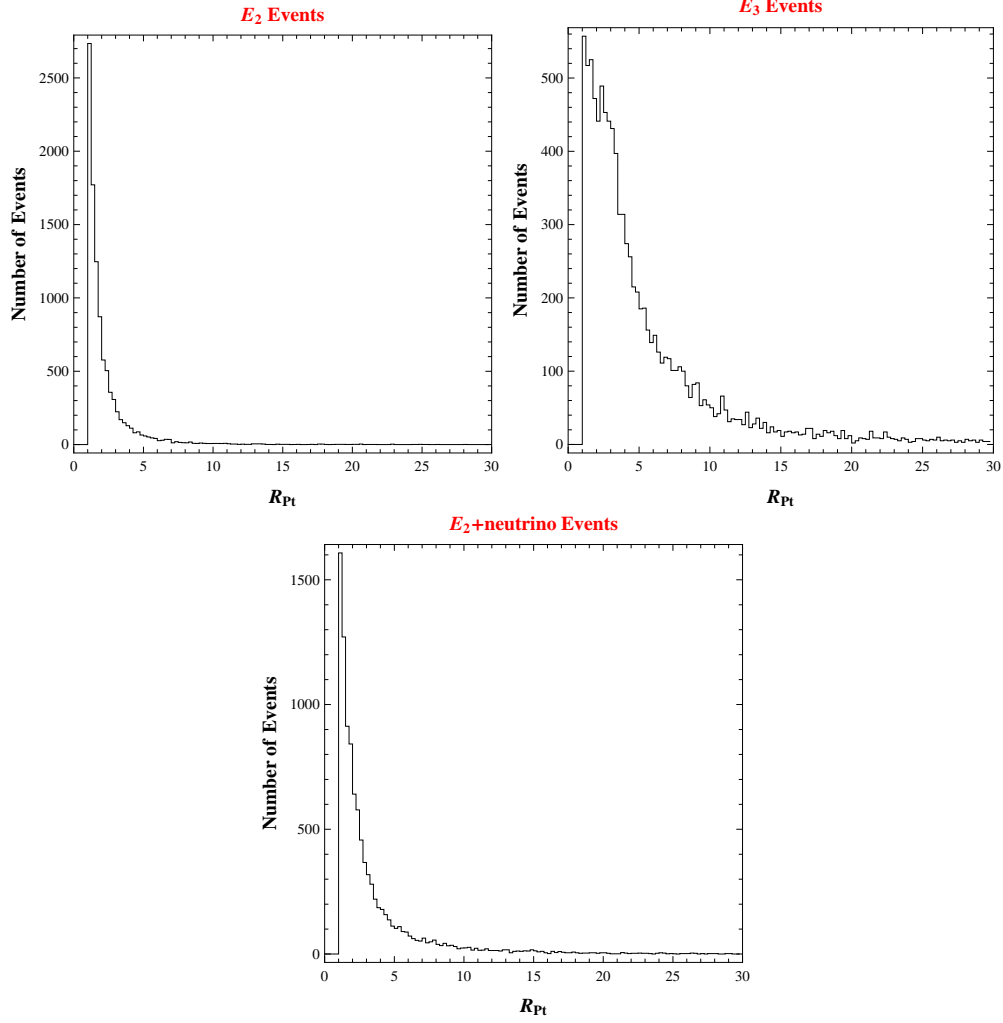[25]We neglect E_4-type events and comment on this issue later.

Figure 6: R_{P_t} distributions for E_2 type events (upper-left panel), E_3 type events (upper-right panel) and $E_2 + \nu$ events (lower panel) for the case with one visible particle on each decay chain. The mother mass is $M = 400$ GeV, the DM mass is $m_{DM} = 150$ GeV.

- if the survival rates for the events (after the R_{P_t} cut) are much larger than that of E_2 values shown in Table 1, then we can conclude that the events are *not* purely E_2 type, i.e., it is an evidence for existence of another/third invisible particle (whether massless or massive).

In general, the survival rates for E_3 type events are much larger than those of E_2 type events, but the survival rates of E_3 type events depend on the mother and DM masses. In addition, the survival rates for $E_2 + \nu$ events are larger than that of E_2 type events as well (even though they are generally smaller than that of E_3 type events). In this sense, an observation of large survival rates might not (by itself) provide a strong support that there exist E_3 type events in the sample.

To get further confirmation of E_3-type events (and thus to distinguish Z_2 and Z_3 models), we can employ the R_{P_t} cut as above and then study the M_{T2} distribution of the *surviving* events. The

key idea is to compare the upper edges of the M_{T2} distributions before and after the R_{P_t} cut. If the underlying physics model is Z_2 type, then clearly we can only obtain E_2 type events (or $E_2 + \nu$) events before and after the cut, and the upper edge of its M_{T2} distribution is not altered. However, if the underlying physics model is Z_3, then (before the cut) the total events are an *admixture* of E_2 and E_3 type. Since the upper edge of E_3 (and E_4)-type events is smaller than those of E_2-type events, the upper edge of M_{T2} distribution (again before the R_{P_t} cut) should be that of E_2 type events. On the other hand, *after* the cut the upper edge of M_{T2} distribution should be lower than before since the surviving events are mostly of E_3 type.

To illustrate this technique, we apply the analysis outlined above to the previously simulated events using a model with $M = 400$ GeV, $m_{DM} = 150$ GeV, and we pick the trial mass to be $\tilde{m} = 25$ GeV for the purpose of illustration. Based on the survival rates shown in Table 1, we choose $R_{P_t}^{\min} = 5$. Before we do the analysis, we need to investigate whether the $R_{P_t} > 5$ cut is "biased", i.e., does the cut tend to remove more events with a high M_{T2} value?[26] For this we consult Fig. 7, which shows *separately* the M_{T2} distributions for both pure E_2 and E_3 type events before and after the R_{P_t} cut. By comparing the left panels and right panels in Fig. 7 we can easily see that the upper edges for both E_2 and E_3 type events do not get modified after the R_{P_t} cut, which suggests that the R_{P_t} cut is not "biased" [27]. In addition, we see that these upper edges in simulated events approximately agree with the theoretical predictions (shown by vertical lines)[28].

Now we can demonstrate how to distinguish Z_2 and Z_3 models using a *combination* of R_{P_t} cut and M_{T2} distributions. First we consider a Z_3 model, where we assume that the branching ratio for the mother to decay into one DM (and visible particle) and into two DMs (and visible particle) are both 50%.[29] Since we assumed that the visible particles in these two decays are identical, we have to combine the M_{T2} distributions for E_2 and E_3 type events in a $1:2$ ratio to get the *total* M_{T2} distribution. The result is shown in the left panel of Fig. 8. As expected, we can see from this figure that the combined E_2 and E_3 type events have an upper edge in M_{T2} distribution that agrees with the theoretical expectation for E_2 type events (the red solid line). As discussed earlier, we can also see that the total M_{T2} distribution has a kink near the theoretical $M_{T2}^{\max}$ for E_3 type events, but it is hard to identify such a kink because of statistical fluctuations. The right panel of Fig. 8 shows the M_{T2} distribution for the combined events *after* the R_{P_t} cut. It can be seen clearly that the upper edge of M_{T2} distribution gets reduced. In fact, the new edge agrees with the theoretical expectation of the $M_{T2}^{\max}$ of E_3 type events (the blue solid line). This confirms our expectation that the R_{P_t} cut discards most of E_2 type events while retaining a sizeable fraction of

---

[26] If the answer is affirmative, then $M_{T2}^{\max}$ after the cut will be reduced even for *purely E_2-type* events.

[27] But a choice of larger $R_{P_t}^{\min}$ would introduce bias in the cut.

[28] But note that in experiments these predictions are *a priori* unknown since we do not know the masses of the mother and DM separately.

[29] In general, the decay into two DM should be phase-space suppressed relative to the decay into one DM. However, in some specific models, this suppression (for the decay chain with two DM) could be compensated by larger effective couplings in that chain so that the two decay processes can have comparable branching ratio as assumed here.
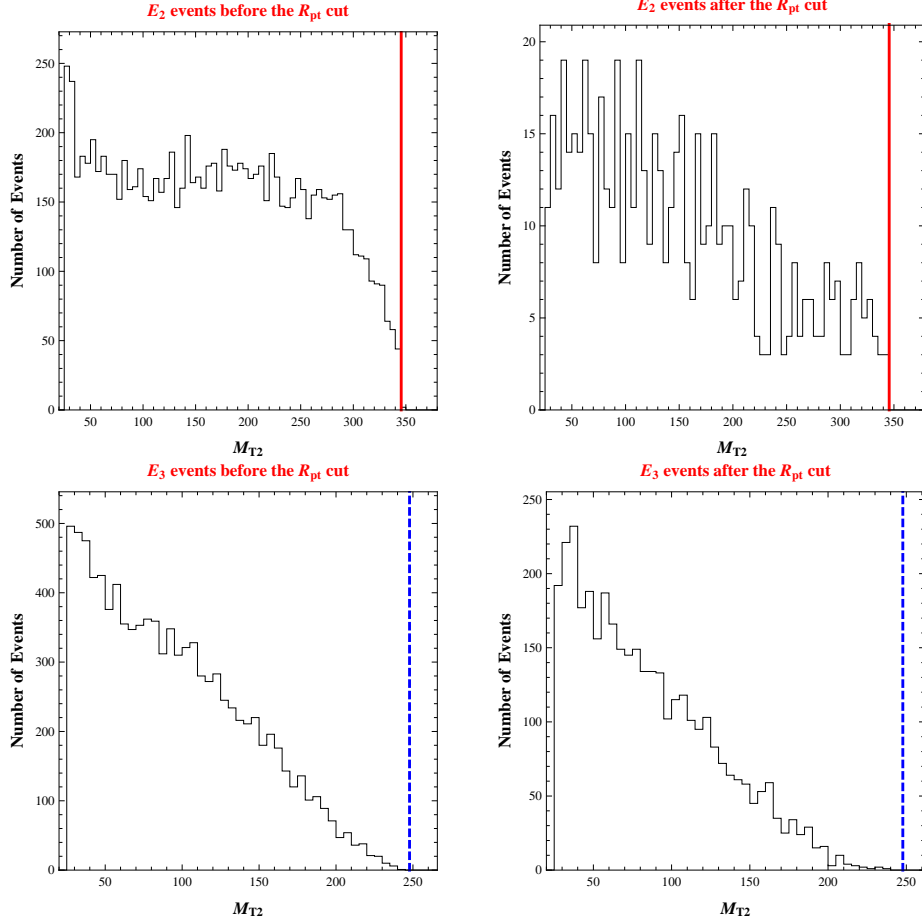
Figure 7: M_{T2} distribution for E_2 (top two panels) and E_3 type events (lower two panels) for simulated events using a model with $M = 400$ GeV and $m_{DM} = 150$ GeV and one visible particle per decay chain. The trial mass is chosen to be $\tilde{m} = 25$ GeV. The left panels are the M_{T2} distributions before the R_{P_t} cut, and the right panels are the M_{T2} distributions after the R_{P_t} cut. The solid red (dashed blue) lines are the theoretical prediction for the upper edges of M_{T2} distribution for E_2 and E_3 type events, respectively.

E_3 type events, i.e., the events which pass the R_{P_t} cut are mostly E_3 type.

Of course, we do not know *a priori* where the $M_{T2}^{\max}$ for E_3 type events (solid blue line) lies due to the lack of knowledge of the mother and DM masses. Rather the idea is that we can simply *measure* the upper edge in M_{T2} distributions after the R_{P_t} cut (again, this approximately correspond to that of E_3-type events). Combining this edge with that before the cut (i.e., corresponding to E_2-type event) then allows us to evaluate the masses of mother and DM particles as described in detail in section 4.1[30]. A complication arises (as follows) in obtaining the $M_{T2}^{\max}$ for events after the R_{P_t} cut. As can be seen in the right panel of Fig. 8, there are still some events beyond the theoretical value of $M_{T2}^{\max}$ for E_3 type events (the blue solid line in the plot), for example from (a small number of)

---

[30]Note that this cannot be done in Z_2 models as discussed in section 4.1.
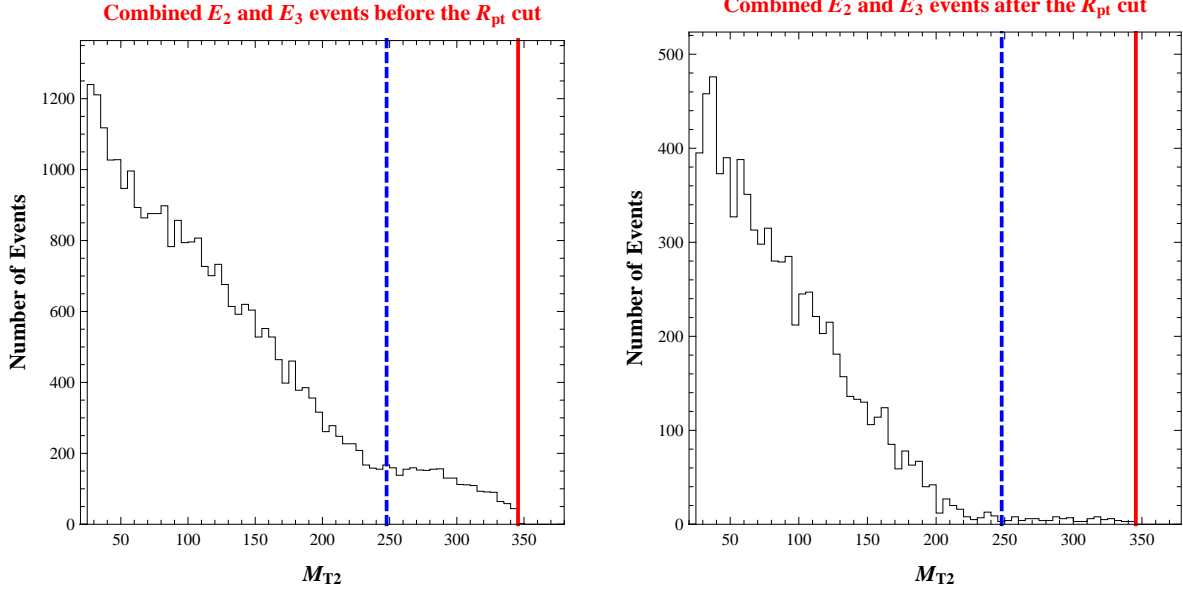
Figure 8: M_{T2} distribution for combined E_2 and E_3 type events $(1 : 2$ ratio) before (left panel) and after (right panel) the $R_{P_t} > 5$ cut for the case with one visible particle per decay chain. The mother mass is $M = 400$ GeV and the DM mass $m_{DM} = 150$ GeV. The trial mass is chosen to be $\tilde{m} = 25$ GeV. The solid red (dashed blue) lines represent the theoretical predictions for the upper edges of M_{T2} distributions for E_2 and E_3-type events, respectively.

E_2-type events which passed the cut. So we need an algorithm to get rid of those "background" events and do a fit to the M_{T2} distribution in order to find $M_{T2}^{\max}$. The details of the method we employed are discussed in App. C. We apply the above techniques to the simulated events. The values of mother and DM masses we obtained from this analysis are 394 ± 8 GeV and 142 ± 13 GeV, which agree quite well with the theoretical values (400 GeV and 150 GeV). However, we expect that uncertainty in energy measurements would introduce additional errors so that a more thorough analysis taking into account these effects (which is beyond the scope of this paper) is needed in order to be more realistic.

For comparison, we consider now Z_2 models. In these models, we have either E_2 or $E_2 + \nu$ events. For pure E_2 type events, we have already shown in the upper panels of Fig. 7 that the upper edge of M_{T2} distribution is not reduced after the R_{P_t} cut (note that this would not be true if the R_{P_t} cut is "biased"). For completeness, we also consider Z_2 models where the mother can decay into one DM or one DM plus neutrino, with the visible particle in the two decay chains being identical. We again assume that both branching ratios are 50%. Thus, we will obtain a *combination* of $E2$ and $E_2 + \nu$-type events. The M_{T2} distributions in this case are shown in Fig. 9. The left panel shows that before the R_{P_t} cut, the upper edge of M_{T2} distribution agrees with the theoretical prediction of E_2 type events and does not have a kink. And, by comparing with the right panels of this figure (i.e., after the R_{P_t} cut, when mostly $E_2 + \nu$-type events survive) we can see that the
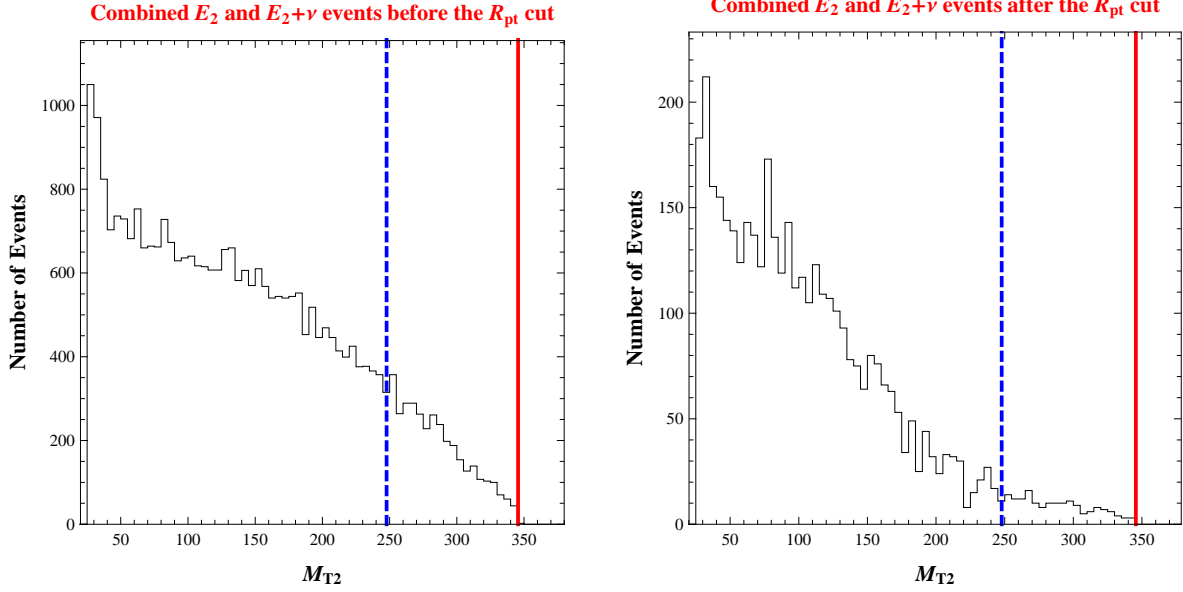
27

Figure 9: M_{T2} distribution for combined E_2 and $E_2 + \nu$ events $(1 : 2$ ratio) before (left panel) and after (right panel) the $R_{P_t} > 5$ cut for the case with one visible particle per decay chain. The mother mass is $M = 400$ GeV and the DM mass $m_{DM} = 150$ GeV. The trial mass is chosen to be $\tilde{m} = 25$ GeV. The solid red (dashed blue) lines represent the theoretical predictions for the upper edges of M_{T2} distributions for E_2 and E_3-type events, respectively.

location of the upper edge for M_{T2} distribution also does not change. These two observations are easily explained by the fact that, as discussed earlier, the $M_{T2}^{\max}$ for $E_2 + \nu$-type events is *same* as for (purely) E_2-type events. Based on the above discussions for Z_2 and Z_3 models, we conclude that

- by observing whether the upper edge of M_{T2} distribution changes (in particular, reduces) *after the R_{P_t} cut*, we can distinguish between Z_2 (including those with neutrino appearing in decay of a mother) and Z_3 models.

5.1.2 More than One Visible/SM Particles in Each decay Chain

Next let us consider the case with more than one visible/SM particles per decay chain[31] To be specific, we consider the case with two visible particles per decay chain. A similar analysis can be done if there are more than two visible particles. To separate E_2 and E_3 type events, we consider the ratio of H_t, where $H_t^i = \sum_a |P_t^{v_a^i}|$ is the scalar sum of P_t's of visible particles in the same decay chain (assuming we know which particles come from which decay chain), and $i = 1, 2$ is the index

---

[31]Note that in this case, we will get a double-edge in the visible invariant mass distribution from a *single* mother decay, which can already be used to distinguish Z_3 from Z_2 models [36]. However, it is always useful to have more techniques – such as the one, using decays of *both* mothers in the event, that we are developing here – for such discrimination.

$R_{H_t}^{\min}$	2	3	4	5	6	7	8	9	10
E_2	0.1542	0.0401	0.0142	0.0065	0.0028	0.0015	0.0009	0.0006	0.0005
E_3	0.7990	0.5181	0.3103	0.1905	0.1228	0.0838	0.0583	0.0422	0.0314
E_2 + neutrino	0.3086	0.1192	0.0551	0.0279	0.0166	0.0104	0.0074	0.0052	0.0035

Table 2: The percentage of survival events in E_2, E_3 type events and $E_2 + \nu$ events for different choice of $R_{H_t}^{\min}$ for the case with two visible particles per decay chain. The mother mass is $M = 400$ GeV and the DM mass is $m_{DM} = 150$ GeV.

for the decay chains. H_t gives a measure of how energetic the visible particles are in each decay chain. We define the H_t ratio as follows

$$R_{H_t} = \frac{H_t^{\max}}{H_t^{\min}}, \tag{34}$$

where $H_t^{\max} = \max(H_t^1, H_t^2)$ and $H_t^{min} = \min(H_t^1, H_t^2)$. From similar reasons to the one visible particle case discussed above, we expect R_{H_t} for E_3 type events to be larger than that for E_2 type events on average. To illustrate this feature, we simulate E_2, E_3 and $E_2 + \nu$ events for a model with $M = 400$ GeV and $m_{DM} = 150$ GeV using MadGraph/MadEvent. The results for the R_{H_t} distribution for different types of events are shown in Fig. 10. It can be seen that these distributions are very similar to the R_{P_t} distributions for the one visible particle case shown in Fig. 6. The R_{H_t} for E_3 type events is on average larger than that of $E_2 + \nu$ events, which in turn is on average larger than that for E_2 type events. The survival rates for E_2, E_3 and $E_2 + \nu$ events for the cut $R_{H_t} > R_{H_t}^{\min}$ with different choices of $R_{H_t}^{\min}$ are shown in Table 2. As in the one visible case discussed before, if the survival rates for the observed events are much larger than the E_2 value shown in Table 2, then we can conclude that the events cannot be purely E_2 type. But large survival rates alone cannot be used as a convincing evidence for Z_3 models.

Just like in the case with one visible particle per decay chain, we again use a combined analysis of R_{H_t} cut and upper edges of M_{T2} distributions to distinguish between Z_2 and Z_3 models. However, there is one major difference between the case with two visible particles per decay chain and the case with one visible particle per decay chain. In the latter case, we cannot find the mother and DM mass just based on the M_{T2} upper edges for events before R_{P_t} cut. On the other hand, in the case at hand, there is a kink structure in the $M_{T2}^{\max}$ vs $\tilde{m}$ plot for E_2-type events events which tells us both the mother and the DM masses (see section 2). And $M_{T2}^{\max}$ for E_3 type events is smaller than that of E_2 type events for $\tilde{m} < m_{DM}$ and the same for $\tilde{m} \geq m_{DM}$ (see section 3.2). Thus, before the R_{H_t} cut, one expects that $M_{T2}^{\max}$ for the *combined* events is always (i.e., irrespective of the trial DM mass) given by that of E_2-type events (just like for the case of one visible particle per decay chain discussed earlier). Therefore, in the present scenario, we can find out the mother and DM masses before we do any R_{H_t} cut. We can then *predict* the edge in M_{T2} for E_3-type events, i.e., after the R_{H_t} cut (again, the events surviving the cut will be mostly E_3-type).
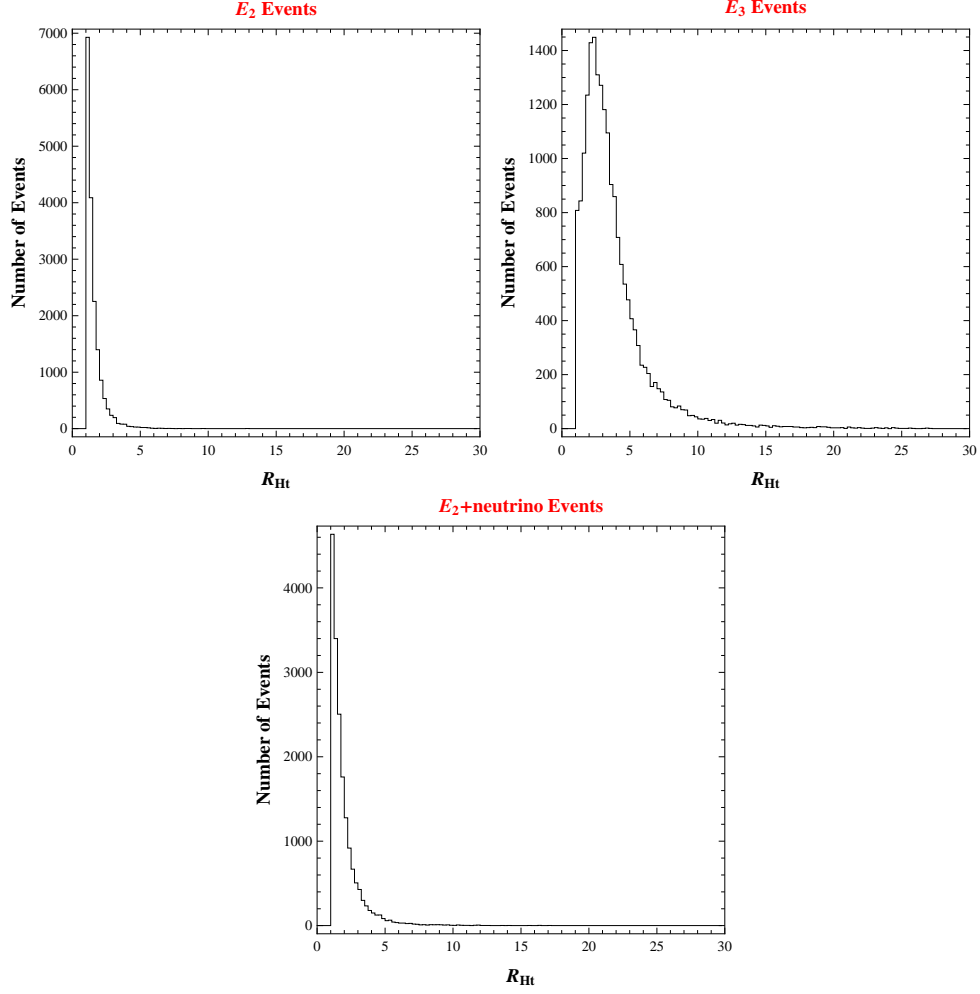
Figure 10: R_{H_t} distributions for E_2 type events (upper-left panel), E_3 type events (upper-right panel) and $E_2 + \nu$ events (lower panel) for the case with two visible particles on each decay chain. The mother mass is 400 GeV, the DM mass is 150 GeV.

We now demonstrate an application of the general strategy outlined above. Based on the survival rates shown in Table 2, we choose $R_{H_t}^{\min} = 3$ in this case. Fig. 11 shows the M_{T2} distributions for the simulated pure E_2 and E_3 type events before and after the R_{H_t} cut. By comparing the left and the right panels in Fig. 11, we can see that R_{H_t} cut does not alter the upper edge of M_{T2} distribution for both E_2 and E_3 type events. Therefore the R_{H_t} cut is not "biased" [32]. We then consider a Z_3 model where the branching ratios of mother decaying into two DMs (plus two visible particles) and into one DM (plus two visible particles) are both 50%. We show the M_{T2} distributions for the combined events before (left panel) and after (right panel) the $R_{H_t} > 3$ cut in Fig. 12. As expected, we see that before the R_{H_t} cut, the upper edge of M_{T2} distribution agrees with the theoretical prediction of E_2 type events (shown by the red line). And, the upper edge for the M_{T2} distribution gets reduced after the R_{H_t} cut[33], which can serve as an evidence for Z_3 model (cf. discussion of Z_2 model below). In addition, as mentioned earlier, knowing the mother and DM masses from the kink in the plot of $M_{T2}^{\max}$ before the cut as a function of trial DM mass , we can predict (shown by the blue line) the upper edge for the M_{T2} distribution for the events that passed the R_{H_t} cut (it is just the theoretical $M_{T2}^{\max}$ for E_3 type events). From the right panel of Fig. 12 we see that

- the observed $M_{T2}^{\max}$ for events that passed the R_{H_t} cut does agree with the *prediction* (cf. one visible particle case above), thus providing additional evidence that the underlying physics model is Z_3.

We can compare the above result with Z_2 models. If we just have pure E_2 type events, then the R_{H_t} cut does not change the upper edge of M_{T2} distribution, as already seen in the upper panels of Fig. 11. As in the one visible particle case, we can also consider the case where there are $E_2 + \nu$ events in addition to E_2 events: we assume that the branching ratios for mother to decay into one DM plus neutrino (plus two visible particles) and into one DM (plus two visible particles) are both 50%. We show the M_{T2} distribution before (left panel) and after (right panel) the R_{H_t} cut for this case in Fig. 13, from which we can see that the upper edge of M_{T2} distribution before the cut agrees with the theoretical prediction for E_2-type events and that it again does not change after the cut (as expected: see similar discussion for the one visible particle case).

5.2   A Summary of the Analysis and its Limitations

Now we summarize the analysis needed to be carried out to distinguish between Z_2 and Z_3 models when the visible particles on each decay chain are identical.

For the case with one visible particle per decay chain:

---

[32]However, a choice of higher $R_{H_t}^{\min}$ will give rise to bias.

[33]Here, we have chosen 9 GeV as the trial DM mass, i.e., (much) smaller than the actual DM mass so that the difference between upper edges of M_{T2} for E_2 and E_3 type events, i.e., the reduction of the edge after cut, is "exaggerated": see section 3.2.
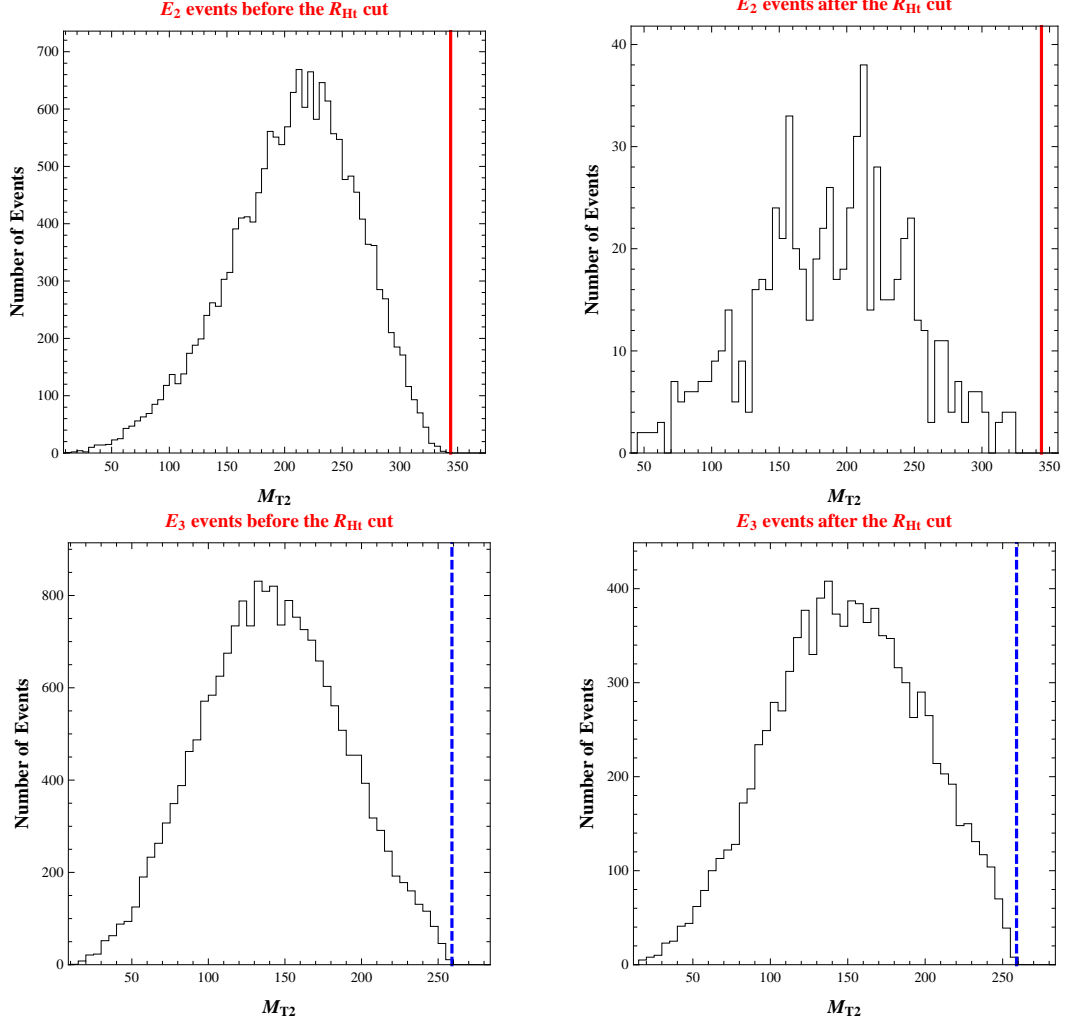
Figure 11: M_{T2} distribution for E_2 (top two panels) and E_3 type events (lower two panels) for simulated events using a model with $M = 400$ GeV and $m_{DM} = 150$ GeV and two visible particles per decay chain. The trial mass is chosen to be $\tilde{m} = 9$ GeV. The left panels are the M_{T2} distributions before the $R_{H_t} > 3$ cut, and the right panels are the M_{T2} distributions after the $R_{H_t} > 3$ cut. The solid red (dashed blue) lines are the theoretical prediction for the upper edges of M_{T2} distribution for E_2 and E_3 type events.
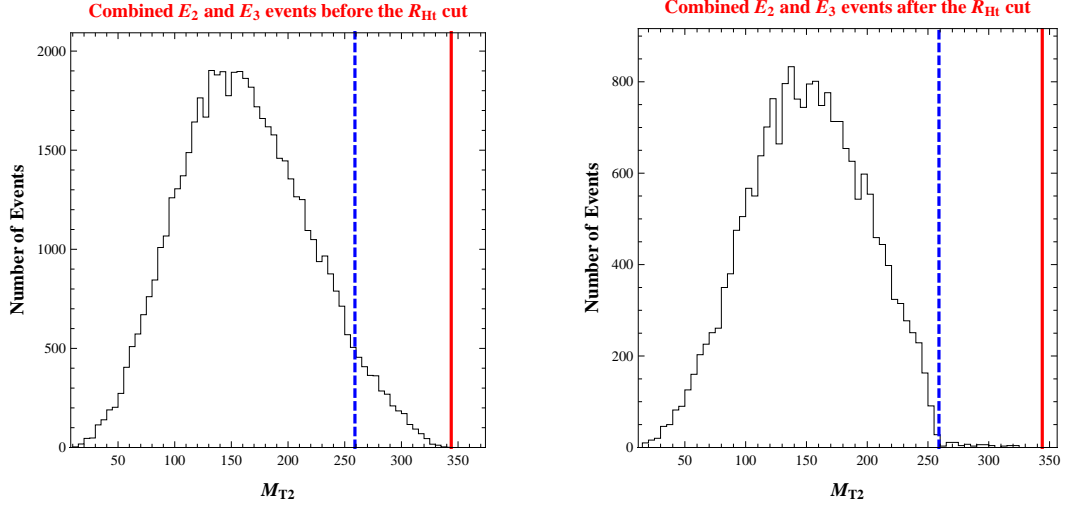
Figure 12: M_{T2} distribution for combined E_2 and E_3 type events ($1:2$ ratio) before (left panel) and after (right panel) the $R_{H_t} > 3$ cut for the case with two visible particles per decay chain. The mother mass is $M = 400$ GeV and the DM mass $m_{DM} = 150$ GeV. The trial mass is chosen to be $\tilde{m} = 9$ GeV. The solid red (dashed blue) lines represent the theoretical predictions for the upper edges of M_{T2} distributions for E_2 and E_3-type events, respectively.

Figure 13: M_{T2} distribution for combined E_2 and $E_2 + \nu$ events ($1:2$ ratio) before (left panel) and after (right panel) the $R_{H_t} > 3$ cut for the case with two visible particles per decay chain. The mother mass is $M = 400$ GeV and the DM mass $m_{DM} = 150$ GeV. The trial mass is chosen to be $\tilde{m} = 9$ GeV. The solid red (dashed blue) lines represent the theoretical predictions for the upper edges of M_{T2} distributions for E_2 and E_3-type events, respectively.
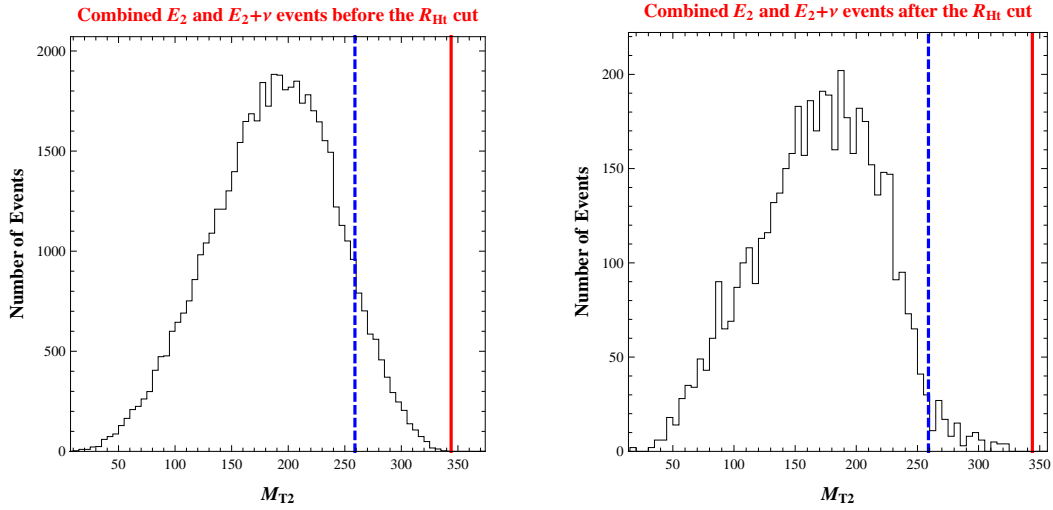
33

- We first find $M_{T2}^{\max}$ with different trial DM masses ($\tilde{m}$) for *all* the events. We can then substitute this value into $\sqrt{C_{E_2}} + \sqrt{C_{E_2} + \tilde{m}^2} = M_{T2}^{\max}$ to find the parameter C_{E_2} (see the details in section 4.1).

- We apply the cut $R_{P_t} > 5$ and find $M_{T2}^{\max}$ with different trial masses ($\tilde{m}$) for the events that passed the cut. If we observe that the $M_{T2}^{\max}$ is reduced *after* the R_{P_t} cut (as compared to before), then we can conclude that the underlying physics model is Z_3 type, otherwise it is Z_2 type. On the other hand, if the $M_{T2}^{\max}$ is not changed after the R_{P_t} cut, then we conclude that the underlying physics model is Z_2 type.

- If we confirmed (as above) that the physics model is Z_3, we can then substitute the $M_{T2}^{\max}$ (for various trial DM masses) for events after the R_{P_t} cut into $\sqrt{C_{E_3}} + \sqrt{C_{E_3} + \tilde{m}^2} = M_{T2}^{\max}$ to find the parameter C_{E_3}. Based on the values of C_{E_2} and C_{E_3}, we can find the mother and DM masses simultaneously (again see the details in section 4.1).

For the case with two visible particles per decay chain:

- We first find $M_{T2}^{\max}$ with different trial masses ($\tilde{m}$) for all events. We then draw a $M_{T2}^{\max}$ versus $\tilde{m}$ plot and find the location of the kink. This can give us both the mother and DM masses.

- We calculate the theoretical predictions of $M_{T2}^{\max}$ for E_3 type events using the mother and DM masses found in the first step.

- We apply the cut $R_{H_t} > 3$ and find $M_{T2}^{\max}$ with different trial masses ($\tilde{m}$) for events that passed the R_{H_t} cut. If the edge in M_{T2} reduces as a result of the cut, then we conclude that the underlying physics model is Z_3. Otherwise, it is a Z_2 model. Furthermore, if the new $M_{T2}^{\max}$ agrees with the theoretical prediction for E_3 type events found in the second step, then we have additional evidence that it is a Z_3 model.

In the above analysis, we have ignored the E_4 type events. However, including these events would not affect our analysis. Specifically, the $M_{T2}^{\max}$ for E_4 type events are always smaller than that of E_2 and E_3 type events (see Eqs. (12) and 20) so that they would not affect the upper edges of M_{T2} distribution for events *both* before and after the R_{P_t}/R_{H_t} cut. However, the survival rates for events after the cuts might be modified. In any case, we did not use the survival rates alone to distinguish between Z_2 and Z_3 models.

The above method of separating E_2 and E_3 type events using R_{P_t} or R_{H_t} cut has its limitations. If the DM mass is very light compared to the mother mass, then the emitted extra DM might not carry away as much energy. Thus, in E_3-type events, the visible particles in the decay chain with two DM particles can be closer (relative to the heavy DM case) in energy to those in the other decay chain. In fact, the DM becomes similar to a neutrino in this case so that the R_{P_t} or R_{H_t}

distributions for E_3 type events should be similar to those for $E_2 + \nu$-type events, in turn, not much different from that of E_2 type events (cf. heavy DM case), and the distinguishing power of the R_{P_t} or R_{H_t} cut is reduced. Therefore, in order for the R_{P_t} or R_{H_t} cut to efficiently separate E_2 and E_3 type events (and hence to distinguish between Z_3 and Z_2 models), we need the mass ratio between DM (m_{DM}) mother (M) masses $\frac{m_{DM}}{M}$ to be sizeable[34].

Finally, we note that the cut on ratio of momentum/energy on the two sides of the full event can also be used – either by itself or in conjunction with edges in M_{T2} – for the non-identical visible particles case (discussed in the previous section) in order to distinguish E_2 and E_3-type events. Of course, in that case, just the *identity* of the visible particles was enough to separate E_3 from E_2-type events.

5.3   Signal Fakes by an (Effective) 2nd DM Particle

Next, we discuss the strategy to distinguish Z_2 models with two different DM particles) from Z_3 models, similar to the discussion in Sec. 4.3. However, now we consider the two decay chains with one and two DM, respectively, in Z_3 models or with the two different DM particles in Z_2 models having identical visible particles (unlike in Sec. 4.3). In this case, there is a modification from the case discussed earlier: we obtain one M_{T2} distribution by simply adding M_{T2} distributions for $E'_{2,\,3,\,4}$-type events in Z_2 models (and similarly, $E_{2,\,3,\,4}$-type events in Z_3 models). Let us consider first the case with a single visible particle per decay chain. As mentioned before, E'_2, E'_3, and E'_4-type events, i.e., "sub"-distributions in the case of Z_2 models, all give a sharp upper edge in the M_{T2} distribution. This observation leads to the expectation of two sharp "kinks" – at the location of the "would-be" (smaller) edges of E'_3, and E'_4-type events – in the middle of the *combined* M_{T2} distribution[35], in addition to the overall upper edge resulting from E'_2 type events.[36].

Note that we had a similar discussion for Z_3 models in the beginning of section 5. However, in the case of Z_3 models only E_2 type events give a sharp upper edge and the other two type events, i.e., E_3 and E_4 give relatively longer tails (albeit with smaller endpoints than E_2-type events) so that two kinks in the combined M_{T2} distribution from E_3 and E_4 type events are not clear. Therefore, clear sharp kink(s) in the M_{T2} distribution would suggest that the events are the result of a Z_2 model (as discussed earlier).

For the case with more than one visible particle in each decay chain, the above idea of using kinks in M_{T2} distribution might fail since edge of the sub-distributions are not sharp, even in the case of Z_2 models (as discussed in section 4.3). Instead, we can do cross-checks like in the case of non-identical visible particle(s) in the two decay chains (discussed in section 4.3) i.e., we first measure the masses of mother and DM particles by examining the location of the kink present in

---

[34]Of course, we need $m_{DM}/M < 0.5$ in order for the decay chain with two DM to be kinematically allowed.

[35]not to be confused with kink in edge of M_{T2} as a function of trial mass!

[36]The situation is similar to the double edge signal in the case of off-shell intermediate particles studied in the reference [36]

the maximum M_{T2} as a function of the trial DM mass for E_2 or E_2'-type events, and then predict the location of edges in the other types of events. Of course, in order to follow this strategy in the present case, one must first separate the events which are mixed, i.e., combination of $E_{2,3,4}$ in the case of Z_3 models and $E_{2,3,4}'$ for Z_2 models, into each individual type by applying P_t/H_t ratio cut (as explained in detail in Sec. 5.1 for Z_3 models). Note that even mixed events in Z_2 models with a second DM-like particle can be separated by P_t/H_t ratio cut because the E_3'-type events also have an imbalance in the energy/momentum of the visible on the two decay chains due to the difference between m_{DM} and m_{DM}'.[37] Of course, we can also do a similar separation for the case of *one* visible particle in each decay chain (which was just discussed above) and then repeat the strategy which we discussed in section 4.3 for the case of visible particle in the two decay chains being non-identical, i.e., consider the shape of the separated M_{T2} distributions in order to distinguish Z_3 from Z_2 models.

6 Future Considerations

6.1 On-Shell Decay Processes

In the previous sections we have focused only on decay chains where the intermediate particles are off-shell. We have used H_T cuts to reduce the inherent Z_2-like background (events with two DM candidates in the final state) to E_3-type events (events with three DM candidates in the final state) for the case when each of the pair produced mothers decay to the *same* SM final state. As a reminder E_3 events do not occur in models with a Z_2 stabilization symmetry. An important question is whether this method can be applied to decays where the intermediate particles are on-shell.

For a quick example on how the decay of the mother particles into intermediate particles that are on-shell can complicate the analysis of the previous section, consider the pair production of mother particles which are charged under a Z_2 stabilization symmetry. We will assume each mother decays via on-shell intermediate particles into a dark matter candidate and identical SM particles. Now suppose the first mother decays into virtual daughters whose mass differences with the each other, the mother and dark matter are large. The second mother decays into intermediate daughters whose mass differences are all small except for one. It is clear, in this latter case, there will be events where the transverse momentum of the visible particles can be small. It is also conceivable, for those events, phase space available to visible particles in the first mother decay is relatively large. In these events, on average, the H_T ratio can be large and therefore can fake the Z_3 signal.

To make this more clear, let us go a step further consider the following explicit example. The

---

[37]Obviously, one cannot then use this cut *on its own* in order to distinguish Z_3 from Z_2 models.
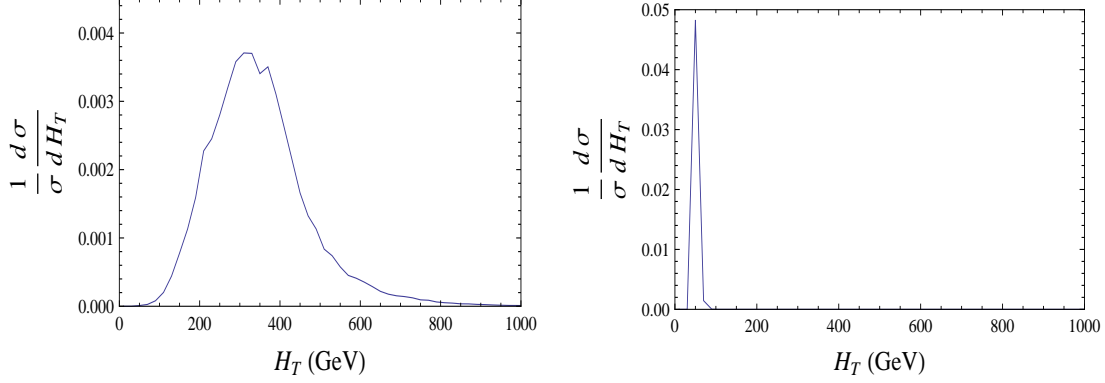
Figure 14: The production and decay of Q in Eqs. (35) and (36). In the panel on the left the intermediate particles generating the decay have a mass difference of 200 GeV. On the panel on the right, all of the mass differences are set to 5 GeV with the exception of one which is 590 GeV. (See Eqs (40) through (42).) The dark matter mass is the same for both plots and is charged under a Z_2 symmetry.

production of two mother particles can be

$$pp \to Q\overline{Q}, \tag{35}$$

where Q is a new, heavy particles. Q and $\overline{Q}$ decay to a final state $Q \to q\bar{l}l\chi$ via the following on-shell intermediate particles

$$
\begin{aligned}
Q &\to A\,q & \overline{Q} &\to A'\,\bar{q} \\
A &\to B\,\bar{l} & A' &\to B'\,l \\
B &\to l\,\chi & B' &\to \bar{l}\,\chi.
\end{aligned}
\tag{36}
$$

Here χ is the dark matter particle, A, A', B and B' are intermediate particles. The lowercase letters are the other SM particles. The important mass differences are

$$\delta m_{QA} = m_Q - m_A \qquad \delta m_{\overline{Q}A'} = m_{\overline{Q}} - m_{A'} \tag{37}$$

$$\delta m_{AB} = m_A - m_B \qquad \delta m_{A'B'} = m_{A'} - m_{B'} \tag{38}$$

$$\delta m_{B\chi} = m_B - m_\chi \qquad \delta m_{B'\chi} = m_{B'} - m_\chi. \tag{39}$$

If the mass differences, δm_{QA}, δm_{AB}, $\delta m_{B\chi}$, are relatively large and the differences, $\delta m_{\overline{Q}A'}$, $\delta m_{A'B'}$, $\delta m_{B'\chi}$, are small then the H_T ratio may be askew. We show this explicitly in Figure 13 for

$$\delta m_{QA} = \delta m_{AB} = \delta m_{B\chi} = 200 \text{ GeV} \tag{40}$$

$$\delta m_{\overline{Q}A'} = \delta m_{A'B'} = 5 \text{ GeV} \tag{41}$$

$$\delta m_{B'\chi} = 590 \text{ GeV}. \tag{42}$$

37

where m_Q = 700 GeV and m_χ = 100 GeV. H_T is plotted above for the small mass and large mass separation cases. This argument is general and can be applied to many on-shell decay scenarios. For this paper, we considered only off-shell decay scenarios. We leave these questions to future work.

6.2   Invisible Z Decay Background Considerations

Beyond the on-shell considerations described above, in future work we will also consider acceptance cuts and detector effects consistent with the ATLAS and CMS experiments. An important irreducible background to our signal with DM in the final state is the emission of Z bosons that decay invisibly. The standard way to mitigate the effect of this background is to look for events which radiate off a Z boson decaying to electrons or muons. These Z bosons can be reconstructed with standard invariant mass techniques. Knowing the Z boson branching fractions, one can then reliably estimate the number of invisible Z boson decay events[38]. To be conservative, we will require the signal cross section, after detector and acceptance cuts, to be more than 10% of this SM background to preclude statistical fluctuations [43].

6.3   Resolving Reconstruction Ambiguities in Multi-Jet Events with Large $\not{E}_T$

Thus far, we have not applied our analysis to many-particle final states with large $\not{E}_T$. Clearly, we want to be able to distinguish E_3 versus E_2 events for those scenarios. The problem is reconstruction ambiguities are inherent in, e.g., multi-jet events. Consider the pair production of mother particles which decay on-shell into a six-jet final state with two SUSY-like dark matter candidates. In order to reconstruct the decay chain, experimentalists must consider 6! = 720 combinations of jets! Such ambiguities can prevent accurate reconstruction of events with dark matter candidates, not to mention distinguishing scenarios with two versus three dark matter particles in the final state. Thus, the question of searching for dark matter in events with many visible final states is **really** the question of finding methods to enable accurate reconstruction.

Consider the difficult case of decay chains with multi-jet final states and large amounts of missing energy. Several groups have proposed methods to increase the efficiency of reconstructing such events [37, 44]. These methods require the final state jets to have large p_T cuts. Because of the large p_T cuts, the regime of phase space where the mother particles are highly boosted is selected. These methods are therefore essentially variants of the aptly named "hemisphere method." By definition, the hemisphere method considers only events where the mother particles are highly boosted. Thus,

---

[38]This technique is common and used often with analysis of estimating the sensitivity ATLAS and CMS to invisible higgs decay processes. See for example [41, 42]. Also, as an additional note, it is conceivable that the techniques introduced in the previous sections can be applied to separate the signal (DM events) from background processes that include invisible Z decays. However, since estimating the invisible Z branching fraction from data as indicated above is straightforward and reliable, we focus on that method.

final state jets resulting from each mother's decay is correlated in different sides of the detector. The correlation allows experimentalists to accurately associate the correct final state jets with the right decay chain. There are, however, inherent problems with this method:

1. New particles produced at the LHC are expected to be heavy and therefore produced dominantly at threshold. Requiring boosted mother particles pushes production into the regime of phase space where the number of signal events are likely to be smaller than that at threshold.

2. Reconstructing multi-jet events requires hard jets with large cone separations ($\Delta R > 0.4$ or 0.5) between the jets. When the jets are correlated in different hemispheres of the detector, this requirement will further reduce the number of events which will pass to become signal.

With the signal events expected to be small (because of the heavy mother production), it is crucial to keep as many of the signal events as possible. Thus, the **true** goal would then be to accurately reconstruct these events with only the acceptance and kinematical cuts needed to identify the signal and reduce the SM background. We now briefly outline [45] a method to reduce the combinatorics needed to reconstruct events with multi-jet final states with large $\not{E}_T$. We also present very preliminary results. The full results will appear in [45]. To simplify the discussion in the next sections, we assume pair production of mother particles with each decaying into identical dark matter candidates plus jets[39].

6.3.1 Proposed Algorithm

The reconstruction algorithm is:

Step 0: Obtain a statistically significant amount of n-jet events (with a large amount of $\not{E}_T$) over the SM background.

Step 1: From these events, first consider only the events that remain in the limit of the hemisphere method, i.e., the final state jets have a large p_T. The number of events retained in this limit must still be statistically significant[40] over the remaining background.

Step 2: In the hemisphere method limit, the topology of the signal events can be obtained.

To make Step 2 clearer, consider the example of a six-jet final state. A visual representation of the topologies is in Figure 15. Again, we assume pair production of mother particles with each decaying into identical dark matter candidates plus the SM; also, in the hemisphere limit, the jets are required to be well separated. If, in the limit of the hemisphere method, one mother preferentially decays into five jets and the other mother decays to only one, then the "5-1" topology can

---
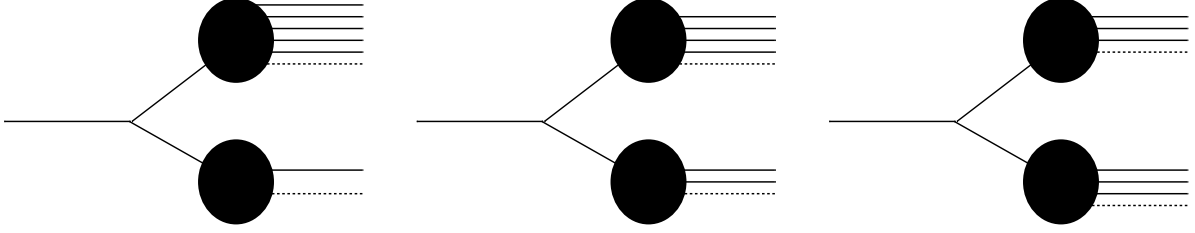
[39]We relax this assumption in [45]

Figure 15: All possible six jet final state topologies with the assumption of pair production of mother particles which decay to the SM and identical DM candidates. The 5-1(left), 4-2 (center) and 3-3 (right) topologies are shown.

be identified. As described in the previous section, the identification is due to the mother particles being boosted; the resulting decay products are therefore on different hemispheres of the detector and can be readily associated with the right decay chain. Another example is possible with one mother decaying into two jets and the other decaying into four jets. This produces a "4-2" topology. Thus, Step 2 is crucial to identify which topology (or combination of topologies[41]) is generated.

> Step 3: In the hemisphere limit, reconstruct the n-jet invariant masses for the topology(-ies) determined in Step 2. This is to find kinematic edges.

It is well known heavy mother decays into the SM and dark matter generate invariant mass "edges." Consider again the case of the 4-2 topology. Reconstructing the four-jet invariant mass associated with the mother decaying to four jets plus dark matter generates an edge. This edge is roughly at $M_{\text{mother}} - M_{\text{dark matter}}$. The measured values of these edges will help to increase the efficiency of reconstructing when going away from the limit of the hemisphere method. We discuss this more detail in the next section. Also, please note, if the decays of a mother is on-shell, even more edges are possible than the ones described above. This will further increase the efficiency of reconstruction. We show an example of a kinematic edge in the next section.

So far the above steps have been done in the limit of the hemisphere method. The next step is new and is our primary point:

> Step 4: Reconstruct all of the events with the topology(-ies) determined in the limit of the hemisphere method. Knowing these topologies serves as a reconstruction template to minimize combinatorics for the events which do not have boosted mother particles.

---

[41]It is possible that multiple signal production processes can generate, e.g., 5-1 and 4-2 topologies. If both topologies are determined, then reconstructing the full data set requires the assumption of both. More details are included in [45]. Also, if e.g., a 4-2 topology is produced, this means events with four and eight jet final states are also produced. By focusing on six jet final states, we do not consider these events.

Thus, our point is the use of the hemisphere method to learn the topologies of the signal event. This in turn, will **reduce the combinatorics** needed to reconstruct the full set of signal events when only the cuts needed to reduce the SM background are applied. Consider again the example of a six jet final state. If, in the limit of the hemisphere method, one mother is found to decay into two jets and the other four jets, the number of ways to associate the jets with the correct decay chain is 15. In the case of the 3-3 and 5-1 topologies, it is 20 and 6, respectively. The invariant mass edges determined in the hemisphere method limit will further help to reduce the possible ways to associate the various jets with each decay chain even further. We describe some specifics briefly in the next section.

6.3.2 Additional Notes on Implementing the Algorithm

To begin, for each event, the jets are labeled by decreasing p_T. Like in the previous sections, the scalar sum of the p_T of several jets, H_T, is defined as

$$H_t = \sum_{a=1}^{j} |P_t^a| \tag{43}$$

for a number of jets, j. We use H_t to go to the limit of hemisphere method. To help associate the correct jets with the right decay chain, we also construct the transverse sphericity (S_T) for n-jets, where n can be less than the total number of final state jets. The number of jets included in the definition depends on the assumed topology for reconstruction. S_T is defined as

$$S_T = \frac{2\lambda_2}{\lambda_1 + \lambda_2} \tag{44}$$

where $\lambda_{1,2}$ are the eigenvalues of the 2×2 sphericity tensor

$$S_{ij} = \sum_{\kappa} p_{\kappa i} \, p^{\kappa j} \tag{45}$$

where κ runs over the number of jets included. In general, when the jets used to compute S_T are collinear or back-to-back, then $S_T \to 0$. Because of this property, S_T is used to help determine the topologies of the signal events in the limit of the hemisphere method[42].

In the previous section, we described how reconstructing invariant masses in the hemisphere limit can help reduce combinatoric ambiguities. We want to give a basic example of how this is possible. Consider again the example of a six-jet final state. Suppose the signal topology is a 5-1 topology. In this example, the signal event is generated by pair production of 700 GeV heavy quarks, Q_H, one of which decays into five jets and 100 GeV scalar dark matter, $\tilde{\chi}$. The other mother decays to only one jet and the same dark matter candidate,

$$p\,p \to \overline{Q}_H\,Q_H \to \bar{q}\,q\;\bar{q}\,q\;\bar{q}\,q\;\tilde{\chi}\,\tilde{\chi}^*. \tag{46}$$

---

[42]Beyond, H_T and S_T other, more common, kinematic variables also will be used identify the topology(-es) in the hemisphere limit. We expand on this in detail in [45].
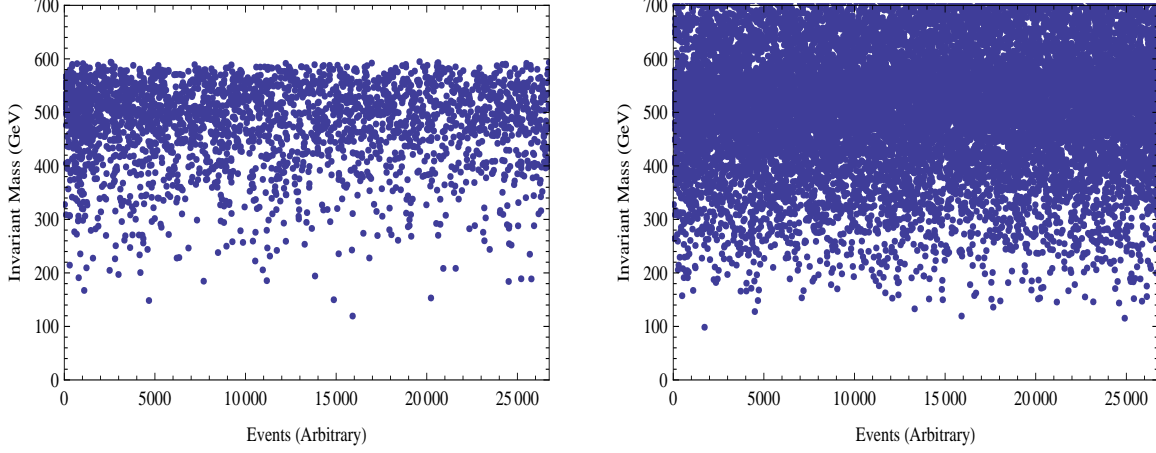
Figure 16: Signal process described in Eq. (46) for a 5-1 topology. The left panel is the five-jet invariant mass in the limit of the hemisphere method. Here the hemisphere method is defined as the cuts in Eq. (47) with the exception that all of jets have $p_T > 150$ GeV. The right panel considers the same events with the cuts in Eq. (47). Note: The reconstruction ambiguities obscure the kinematic edge. All of the events above the 600 GeV edge are events with poor reconstruction.

The virtual particles which contribute to the five-jet decay chain have the masses of 580, 460, 340 and 220 GeV. The five-jet invariant mass has a kinematic edge at approximately $M_{Q_H} - M_{\tilde{\chi}} = 600$ GeV. In the left panel of Figure 16, we plot the five-jet invariant mass in the limit of the hemisphere method. Each dot represents an event. It is clear an edge has appeared at 600 GeV. In the right panel, we plot the same five-jet invariant mass with only the cuts needed to reduce the SM backgrounds:

$$p_{T \text{ leading jet}} > 100 \, \text{GeV} \qquad p_{T \text{ non–leading jets}} > 50 \, \text{GeV}$$
$$|\eta_{\text{jets}}| < 2.5 \qquad \qquad \not{E}_T > 100 \, \text{GeV} \qquad (47)$$
$$S_{T \text{ all jets}} > 0.2 \qquad \qquad \not{E}_T > 0.2 \, M_{\text{eff}}$$
$$\Delta R_{jj} > 0.4$$

where effective mass is defined as

$$M_{\text{eff}} = \sum p_{T \text{ jets}} + \not{E}_T. \qquad (48)$$

This cuts are consistent with the ATLAS and CMS collaborations. With only these cuts, we have reconstructed the multi-jet events assuming the 5-1 topology determined in the limit of the hemisphere method. The key point is the edge determined in the hemisphere method limit means all of the invariant masses greater than 600 GeV are mis-reconstructions. As described above, the amount of mis-reconstructions can be further eliminated if the decay is on-shell and all possible kinematic edges are applied. At the partonic level, the reconstruction efficiency for on-shell decays for the above example approaches 80% [45].

42

The next steps to optimize this method is to include QCD backgrounds as well as a variety of signal processes with virtual particles different spins. A major fault with Figure 16 is that it was generated at the partonic level. The final study [45] should put the signal processes through pythia to get an estimate of hadronization effects.

7 Conclusions and Outlook

The LHC experimental program is ramping up. One of its goals is to test the idea of a WIMP as a DM candidate, especially one which arises as part of an extension of the SM at the TeV scale. The basic idea is that there is a new (global) symmetry under which the SM particles are neutral, but some of the new particles are charged. Thus, the lightest of these charged particles is stable and under certain circumstances – it certainly has to be electrically and color neutral – can be a DM candidate.

In general, such an extension of the SM also has other (heavier, but still TeV mass) particles which are charged under both the new symmetry *and* under the SM gauge symmetries (especially color). So, these DM "partners" (in the sense that they are charged under the symmetry which stabilizes DM) can be copiously produced at the LHC. In turn, these DM partners (or "mother" particles) will decay into SM particles and DM, resulting in events with missing energy and jets/leptons/photons. The goal then would be to piece together the details of the DM model, including mass of the DM and the mother particles, by reconstructing the decay chains which lead to such events.

Clearly, the nature of the DM stabilization symmetry plays a crucial role in the above program, in part because it determines the number of DM particles in each decay chain of the mother particle: for example, in the case where a Z_2/parity symmetry stabilizes the DM (typically) only one DM appears in decay of a single mother, whereas in a Z_3 model, both two and one DM are allowed. Of course, each event must necessarily involve two such mothers being produced.

With the above background, in this paper, we showed how to distinguish models with Z_3 DM stabilization symmetry from Z_2. Since earlier work [36] only studied measurements of the *visible* part of a *single* mother decay, here we focussed on using the information from *both* mother decays, including the *missing* energy in the event which is shared between the two decay chains (or sides). We found that the variable $M_{T\,2}$ is useful for this purpose. For simplicity, we studied pair production of the same mother, followed by decays to SM particles and DM which involve only *off*-shell intermediate particles (i.e., which are heavier than their mother particle). Furthermore, we assumed that we know the division the SM particles in the full event into two groups corresponding to each mother [but of course we do not know (a priori) how many DM are in each decay chain].

Clearly, in a Z_3 model, the events can be classified into three types depending on the total

number of DM particles (i.e., two, three or four) vs. only two DM particles for Z_2 model. We showed that the edges of the M_{T2} distributions are different in these three types of events in a Z_3 model, again even if the same mother is produced (vs. only one edge for Z_2 model). This feature allowed us to distinguish Z_3 from Z_2 models. Moreover, we gave predictions for the values of the edges in the two *new* cases, namely three and four DM in each event, as functions of mother and DM mass. Thus, we can extract the mother and DM masses *separately* using the measurements of these different edges for a Z_3 model. This achievement is especially noteworthy for the case of *single* visible particle in each decay chain since a similar measurement of the mother and DM masses is not possible in a Z_2 model, based solely on using M_{T2} variable.[43]

We emphasized that there are two subcases in the above analysis, namely the visible particles in the decay chain with one DM being identical or different (respectively) to those in the decay chain with two DM (for Z_3 models). In the case of the visible particles *not* being identical, it is easy to separate the events of the three types mentioned above so that one can then plot the respective M_{T2} distributions. However, in the case of the visible particles being identical, one obviously has only a *single M_{T2}* distribution (i.e., combination of the above three types) to begin with. Therefore, we developed a new method to separate out the candidate events with three DM vs. two DM in this case, using the observation that the visible particles on the side with two DM will have smaller energy/momentum that the visible particles on the side with one DM in the same event. This feature is to be compared to the visible energy/momentum being more "balanced" in the case of one DM on each side.

We observed that the above imbalance in the energy/momentum on the two sides *by itself* provides a hint for the appearance of three DM in the event. However, combining it with edges in M_{T2} distributions provides a more powerful discriminator. Finally, we briefly mentioned the case of intermediate particles in the decay chain being on-shell.

Signal Fakes: We pointed out that models with Z_2 as a dark matter stabilization symmetry can fake the *three* decay topologies arising in Z_3 models. An example of such a fake comes from the decays in Z_2 models which involve *effectively* a second DM particle (denoted by DM′), for example, a heavier, neutral Z_2-odd, but collider stable particle. In such a Z_2 model, three decay topologies are possible if the pair-produced mother can decay into either DM or DM′, i.e., we can have DM in one side and DM′ on the other side, DM on both sides or DM′ on both sides. Nevertheless, we suggested how to discriminate Z_2 and Z_3 models by using various strategies.

Another possibility for a fake of Z_3-like signals by a Z_2 model comes from pair-production of *more than one* type of mother particles which decay into visible particles and, for simplicity, a single DM particle. Since the upper edge of M_{T2} distributions depend on the mass of the mother particle, the introduction of different types of mother particles can easily generate different locations of

---

[43]The exception to this rule for Z_2 model is when the total transverse momentum of the two mother particles is *non*-zero (for example, due to initial/final state radiation).

upper edges so that it could instead be mistaken as the multiple decay topologies of a Z_3 model (again, with single DM particle). This type of degeneracy between Z_2 and Z_3 models, however, can be easily resolved by taking into account the fact that each event in such a Z_2 model is still "balanced" in the energy/momentum of visible particles on the two sides (again, assuming that there is no second DM-like particle) while events in Z_3 models can have imbalance if they involve one DM on one side and two DM on the other.

Obviously, this and the earlier work [36] are to be viewed as the first steps in the broad program of distinguishing various DM stabilization symmetries using collider data. To this end, we outlined some future steps to implement this program. We leave more detailed studies along these lines, including relaxing some of the assumptions outlined above and further studying various experimental issues, for future work.

Acknowledgements

References

[1] See, for example, G. Bertone, D. Hooper and J. Silk, Phys. Rept. **405**, 279 (2005) [arXiv:hep-ph/0404175].

[2] C. G. Lester and D. J. Summers, Phys. Lett. B **463**, 99 (1999) [arXiv:hep-ph/9906349];

[3] A. J. Barr, C. G. Lester, M. A. Parker, B. C. Allanach and P. Richardson, JHEP **0303**, 045 (2003) [arXiv:hep-ph/0208214]; A. Barr, C. Lester and P. Stephens, J. Phys. G **29**, 2343 (2003) [arXiv:hep-ph/0304226].

[4] W. S. Cho, K. Choi, Y. G. Kim and C. B. Park, Phys. Rev. Lett. **100**, 171801 (2008) [arXiv:0709.0288 [hep-ph]] and JHEP **0802**, 035 (2008) [arXiv:0711.4526 [hep-ph]].

[5] B. Gripaios, JHEP **0802**, 053 (2008) [arXiv:0709.2740 [hep-ph]]; A. J. Barr, B. Gripaios and C. G. Lester, JHEP **0802**, 014 (2008) [arXiv:0711.4008 [hep-ph]].

[6] A. J. Barr, B. Gripaios and C. G. Lester, JHEP **0911**, 096 (2009) [arXiv:0908.3779 [hep-ph]].

[7] C. Lester and A. Barr, JHEP **0712**, 102 (2007) [arXiv:0708.1028 [hep-ph]].

[8] H. C. Cheng and Z. Han, JHEP **0812**, 063 (2008) [arXiv:0810.5178 [hep-ph]].

[9] M. Burns, K. Kong, K. T. Matchev and M. Park, JHEP **0903**, 143 (2009) [arXiv:0810.5576 [hep-ph]]; P. Konar, K. Kong, K. T. Matchev and M. Park, Phys. Rev. Lett. **105**, 051802 (2010) [arXiv:0910.3679 [hep-ph]]; K. T. Matchev and M. Park, arXiv:0910.1584 [hep-ph].

[10] P. Konar, K. Kong, K. T. Matchev and M. Park, JHEP **1004**, 086 (2010) [arXiv:0911.4126 [hep-ph]].

[11] M. M. Nojiri, Y. Shimizu, S. Okada and K. Kawagoe, JHEP **0806**, 035 (2008) [arXiv:0802.2412 [hep-ph]]; M. M. Nojiri, K. Sakurai, Y. Shimizu and M. Takeuchi, JHEP **0810**, 100 (2008) [arXiv:0808.1094 [hep-ph]]; W. S. Cho, W. Klemm and M. M. Nojiri, arXiv:1008.0391 [hep-ph]; M. M. Nojiri and K. Sakurai, arXiv:1008.1813 [hep-ph].

[12] D. R. Tovey, JHEP **0804**, 034 (2008) [arXiv:0802.2879 [hep-ph]]; G. Polesello and D. R. Tovey, JHEP **1003**, 030 (2010) [arXiv:0910.0174 [hep-ph]].

[13] W. S. Cho, J. E. Kim and J. H. Kim, Phys. Rev. D **81**, 095010 (2010) [arXiv:0912.2354 [hep-ph]].

[14] A. J. Barr, C. Gwenlan, C. G. Lester and C. J. S. Young, arXiv:1006.2568 [hep-ex].

[15] M. Serna, JHEP **0806**, 004 (2008) [arXiv:0804.3344 [hep-ph]].

[16] T. Cohen, E. Kuflik and K. M. Zurek, JHEP **1011**, 008 (2010) [arXiv:1003.2204 [hep-ph]].

[17] H. C. Cheng, J. F. Gunion, Z. Han, G. Marandella and B. McElrath, JHEP **0712**, 076 (2007) [arXiv:0707.0030 [hep-ph]]. H. C. Cheng, D. Engelhardt, J. F. Gunion, Z. Han and B. McElrath, Phys. Rev. Lett. **100**, 252001 (2008) [arXiv:0802.4290 [hep-ph]]; H. C. Cheng, J. F. Gunion, Z. Han and B. McElrath, Phys. Rev. D **80**, 035020 (2009) [arXiv:0905.1344 [hep-ph]]; H. C. Cheng, Z. Han, I. W. Kim and L. T. Wang, arXiv:1008.0405 [hep-ph]; Y. Bai and H. C. Cheng, arXiv:1012.1863 [hep-ph].

[18] M. Burns, K. Kong, K. T. Matchev and M. Park, JHEP **0810**, 081 (2008) [arXiv:0808.2472 [hep-ph]]. P. Konar, K. Kong and K. T. Matchev, JHEP **0903**, 085 (2009) [arXiv:0812.1042 [hep-ph]]; P. Konar, K. Kong, K. T. Matchev and M. Park, arXiv:1006.0653 [hep-ph].

[19] M. M. Nojiri, K. Sakurai and B. R. Webber, JHEP **1006**, 069 (2010) [arXiv:1005.2532 [hep-ph]].

[20] B. Webber, JHEP **0909**, 124 (2009) [arXiv:0907.5307 [hep-ph]].

[21] T. Han, I. W. Kim and J. Song, arXiv:0906.5009 [hep-ph]; I. W. Kim, Phys. Rev. Lett. **104**, 081601 (2010) [arXiv:0910.1149 [hep-ph]].

[22] D. R. Tovey, JHEP **1011**, 148 (2010) [arXiv:1008.3837 [hep-ph]].

[23] A. J. Barr and C. G. Lester, arXiv:1004.2732 [hep-ph].

[24] A. J. Barr, B. Gripaios and C. G. Lester, JHEP **0907**, 072 (2009) [arXiv:0902.4864 [hep-ph]].

[25] For a review of supersymmetric DM, see, for example, G. Jungman, M. Kamionkowski and K. Griest, Phys. Rept. **267**, 195 (1996) [arXiv:hep-ph/9506380].

[26] H. S. Lee, Phys. Lett. B **663**, 255 (2008) [arXiv:0802.0506 [hep-ph]].

[27] H. C. Cheng and I. Low, JHEP **0309**, 051 (2003) and JHEP **0408**, 061 (2004) [arXiv:hep-ph/0405243].

[28] G. Servant and T. M. P. Tait, Nucl. Phys. B **650**, 391 (2003); H. C. Cheng, J. L. Feng and K. T. Matchev, Phys. Rev. Lett. **89**, 211301 (2002) [arXiv:hep-ph/0207125].

[29] K. Agashe, A. Falkowski, I. Low and G. Servant, JHEP **0804**, 027 (2008).

[30] D. G. E. Walker, arXiv:0907.3146 [hep-ph].

[31] D. G. E. Walker, arXiv:0907.3142 [hep-ph].

[32] K. Agashe and G. Servant, Phys. Rev. Lett. **93**, 231805 (2004) [arXiv:hep-ph/0403143]. K. Agashe and G. Servant, JCAP **0502**, 002 (2005) [arXiv:hep-ph/0411254]; K. Agashe, K. Blum, S. J. Lee and G. Perez, Phys. Rev. D **81**, 075012 (2010) [arXiv:0912.3070 [hep-ph]].

[33] E. Ma, Phys. Lett. B **662**, 49 (2008) [arXiv:0708.3371 [hep-ph]].

[34] B. Batell, arXiv:1007.0045 [hep-ph].

[35] F. D'Eramo and J. Thaler, arXiv:1003.5912 [hep-ph].

[36] K. Agashe, D. Kim, M. Toharia and D. G. E. Walker, Phys. Rev. D **82**, 015007 (2010) arXiv:1003.0899 [hep-ph].

[37] A. Rajaraman and F. Yu, arXiv:1009.2751 [hep-ph].

[38] J. Alwall *et al.*, JHEP **0709**, 028 (2007) [arXiv:0706.2334 [hep-ph]].

[39] E. Byckling and K. Kajantie, Particle Kinematics (John Wiley & Sons, 1973).

[40] For some recent studies, see, for example, K. M. Zurek, Phys. Rev. D **79**, 115002 (2009) [arXiv:0811.4429 [hep-ph]]; F. Chen, J. M. Cline and A. R. Frey, Phys. Rev. D **80**, 083516 (2009) [arXiv:0907.4746 [hep-ph]]; D. Feldman, Z. Liu, P. Nath and G. Peim, Phys. Rev. D **81**, 095017 (2010) [arXiv:1004.0649 [hep-ph]]; M. Cirelli and J. M. Cline, arXiv:1005.1779 [hep-ph].

[41] The ATLAS Collaboration, CERN-LHCC-99-015.

[42] The CMS Collaboration, J. Phys. G: Nucl. Part. Phys. 34 995-1579 (2007).

[43] Private conversation with M. Shapiro and I. Hinchliffe.

[44] Y. Bai, H. -C. Cheng, JHEP **1106**, 021 (2011). [arXiv:1012.1863 [hep-ph]].

[45] D. G. E. Walker, et al., to appear.

A The location of $M_{T2}^{\max}$

In this appendix we will derive the analytic expression for the location of the upper edge in the M_{T2} distribution. We begin with deriving the general expression of the M_{T2} solution for a given set of kinematic configuration, then move on to obtaining the maxima of the balanced/unbalanced M_{T2} solutions, and close with giving the global maximum of the M_{T2} distribution, followed by a simple application.

A.1 The General Expression for the M_{T2} Solution

The usual M_{T2} variable [2, 3] is defined as a generalized transverse mass such that each of pair-produced mother particles decays into visible particles and one dark matter particle of the same type. However, we do not restrict ourselves to such cases, i.e., we extend our consideration to the cases with more than two DM in a full decay chain (e.g., E_3 and E_4 type events in Z_3 models). Nevertheless, in the analysis of M_{T2} variable, we still *hypothesize* that two dark matter particles with equal mass (i.e., one DM per chain) are involved in the full decay process, i.e., we employ the "naive" M_{T2} method (as mentioned at the beginning of section 3).

The left diagram of Fig. 17 illustrates the decay process of pair-produced mother particles that we are taking into consideration. Here the "blob" denotes off-shell intermediate particles or an (on-shell) point interaction. The red dashed lines represent any particles charged under dark matter stabilization symmetry whereas the black solid lines represent any visible/SM particles. M is the mass of the mother particle, which must be charged under DM stabilization symmetry. As mentioned above, each mother particle can decay into the multiple number of invisible/DM particles as well as the multiple number of visible/SM particles, and this extended possibility is explicitly depicted by the multiple number of red dashed and black solid arrows behind the two small blobs. Each visible/invisible multi-particle state can be collapsed effectively to a(n) visible/invisible single particle state by introducing invariant (transverse) mass, which will be manifest in the detailed formulae later. In this sense, $m_v^{(a)}$ and $m_i^{(a)}$ can be understood as the total invariant masses formed by visible or invisible particles belonging to the same decay chain.

For defining the M_{T2} variable one should be noted that we are not aware of the DM mass in advance. Hence, the best we can do is to introduce trial DM mass. Since we perform the naive
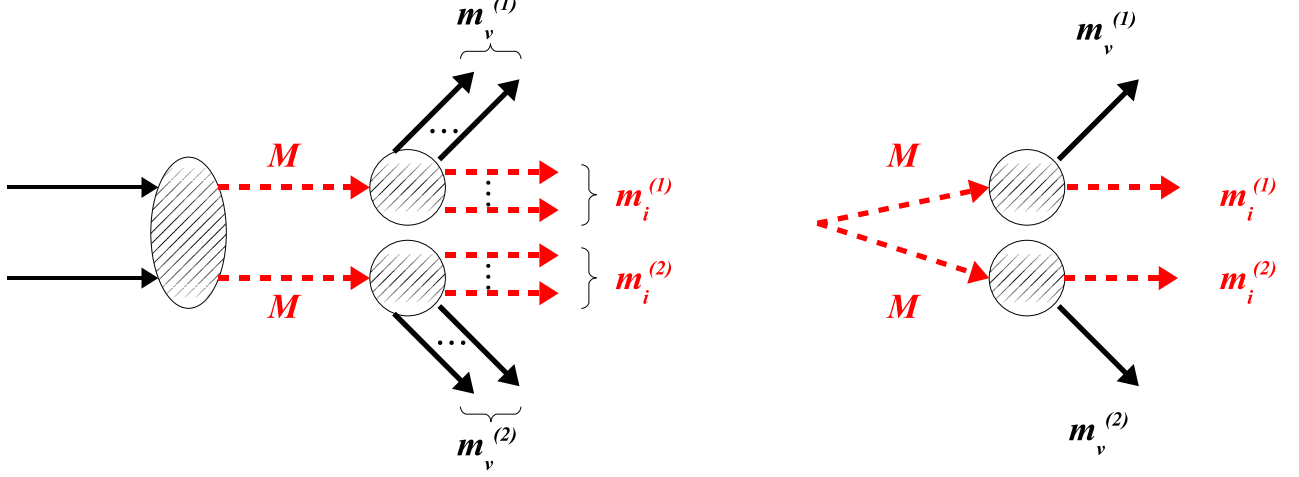
Figure 17: The left panel illustrates the decay process of interest which pair-produced mother particles go through. M, $m_v^{(a)}$, and $m_i^{(a)}$ ($a = 1, 2$) denote the mass of mother particle, total invariant masses of visible particles and invisible particles in the same decay chain, respectively. The right panel illustrates the effective configuration of such a decay process.

M_{T2} analysis as mentioned above, i.e., we assume a single type of DM in each decay chain even if the actual physics could be different, we employ only one type of trial DM mass $\tilde{m}$ and construct the M_{T2} variable as follows [2, 3]:

$$M_{T2}\left(\mathbf{p}_T^{v(1)}, m_T^{v(1)}, \mathbf{p}_T^{v(2)}, m_T^{v(2)}; \tilde{m}\right) \equiv \min_{\mathbf{p}_T^{v(1)}+\mathbf{p}_T^{v(2)}+\tilde{\mathbf{p}}_T^{(1)}+\tilde{\mathbf{p}}_T^{(2)}=0}\left[\max\left\{M_T^{(1)}, M_T^{(2)}\right\}\right] \tag{49}$$

Here each transverse mass of the decay product $M_T^{(a)}$ ($a = 1, 2$) is given by

$$\left(M_T^{(a)}\right)^2 = \left(m_T^{v(a)}\right)^2 + \tilde{m}^2 + 2\left(E_T^{v(a)}\tilde{E}_T^{(a)} - \mathbf{p}_T^{v(a)} \cdot \tilde{\mathbf{p}}_T^{(a)}\right) \tag{50}$$

where $m_T^{v(a)}$, $\mathbf{p}_T^{v(a)}$, and $E_T^{v(a)}$ are the total transverse invariant mass, transverse momentum, and transverse energy of visible particles:

$$\left(m_T^{v(a)}\right)^2 = \left(t_1^{v(a)} + \cdots + t_n^{v(a)}\right)^2 = \sum_\alpha \left(m_\alpha^{v(a)}\right)^2 + 2\sum_{\alpha>\beta}\left(E_{\alpha T}^{v(a)}E_{\beta T}^{v(a)} - \mathbf{p}_{\alpha T}^{v(a)} \cdot \mathbf{p}_{\beta T}^{v(a)}\right) \tag{51}$$

$$\mathbf{p}_T^{v(a)} = \sum_\alpha \mathbf{p}_{\alpha T}^{v(a)} \tag{52}$$

$$E_T^{v(a)} = \sum_\alpha E_{\alpha T}^{v(a)}, \tag{53}$$

and $\tilde{\mathbf{p}}_T^{(a)}$ and $\tilde{E}_T^{(a)}$ are the transverse momentum and energy of the (assumed-to-be-one) *trial* DM particle in each decay chain. Here $m_\alpha^{v(a)}$ indicates the mass of αth visible particle in ath decay chain ($a = 1, 2$) and $t_l^{v(a)}$ indicates the (1+2) momentum on the transverse plane which is defined as

$$t_l^{v(a)} \equiv \left(E_{lT}^{v(a)}, \mathbf{p}_{lT}^{v(a)}\right) = \left(\sqrt{\left(\mathbf{p}_{lT}^{v(a)}\right)^2 + \left(m_l^{v(a)}\right)^2}, \mathbf{p}_{lT}^{v(a)}\right), \tag{54}$$
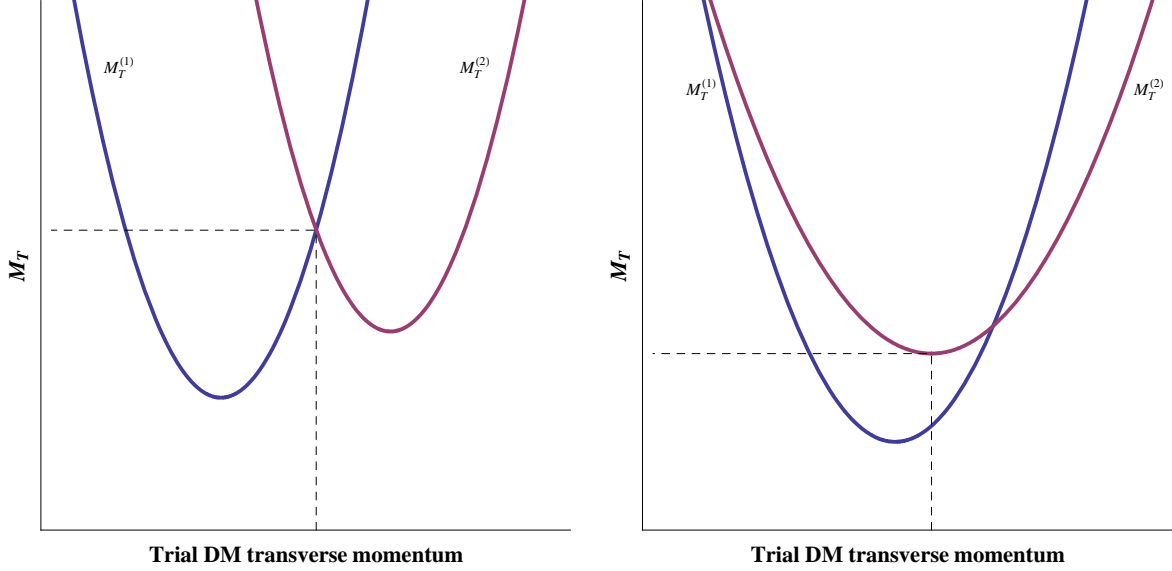
49

Figure 18: Graphical configurations to give rise to a balanced M_{T2} solution (the left panel) and an unbalanced M_{T2} solution (the right panel). The dashed line indicates the solution for the M_{T2} variable to take.

and the metric for this type of momentum is $\mathrm{diag}(1, -1, -1)$. There arise two noteworthy things:

- As far as the range is concerned, the transverse and the regular invariant masses have the same lower and upper limits. Moreover, since the M_{T2} solutions of interest arise at either of the two limits, one may consider the M_{T2} where $m_T^{v(a)}$ are replaced by the regular invariant masses of visible particles $m_v^{(a)}$:

$$\left(m_v^{(a)}\right)^2 = \left(p_1^{v(a)} + \cdots + p_n^{v(a)}\right)^2 = \sum_\alpha \left(m_\alpha^{v(a)}\right)^2 + 2 \sum_{\alpha > \beta} \left(E_\alpha^{v(a)} E_\beta^{v(a)} - \mathbf{p}_\alpha^{v(a)} \cdot \mathbf{p}_\beta^{v(a)}\right). \qquad (55)$$

- As advertised earlier, the entire visible states in the same decay chain can be understood effectively as a single visible particle whose "effective" mass is given by $m_v^{(a)}$. On the other hand, the corresponding "effective" quantity for invisible particles $m_i^{(a)}$ does not seem to be contained in the M_{T2} variable. In fact, the M_{T2} variable depends *implicitly* on $m_i^{(a)}$, which will be cleared shortly.

From these two observations we can reduce the decay of pair-produced mother particles into two multi-particle states (left panel of Fig. 17) to an effective kinematic configuration where there exist two simple 2-body decay chains shown in the right panel of Fig. 17.

For such M_{T2}, there are two types of solution which are called the "balanced" M_{T2} solution and the "unbalanced" M_{T2} solution, and the fact that there always exist some events to give such solutions was proven [2, 3, 4]. The balanced solution arises when $M_T^{(a)} \geq M_T^{(b)}$ for both $a(= 1, 2)$ with the trial DM momentum having the value to accommodate $M_T^{(b)}$ ($b \neq a$) at their global (or

50

so-called "unconstrained") minimum which will be defined shortly (see the left panel of Fig. 18), and otherwise, the unbalanced solution arises (see the right panel of Fig. 18).[44] The global minima for $M_T^{(1)}$ and $M_T^{(2)}$ are easily evaluated by differentiating Eq. (50) with respect to the trial DM momentum and finding the stationary point [2, 3]:

$$\left(M_T^{(1)}\right)_{\min} = m_v^{(1)} + \tilde{m} \tag{56}$$

$$\left(M_T^{(2)}\right)_{\min} = m_v^{(2)} + \tilde{m} \tag{57}$$

The balanced and the unbalanced M_{T2} solutions for a given set of the "effective" visible and invisible masses which are shown in the right panel of Fig. 17 are as follows [2, 3, 4]:

$$\left(M_{T2}^{bal}\right)^2 = \tilde{m}^2 + A + \sqrt{\left(1 + \frac{4\tilde{m}^2}{2A - \left(m_v^{(1)}\right)^2 - \left(m_v^{(2)}\right)^2}\right)\left(A^2 - \left(m_v^{(1)} m_v^{(2)}\right)^2\right)} \tag{58}$$

$$M_{T2}^{unbal} = \tilde{m} + m_v^{(a)} \quad (a = 1, 2) \tag{59}$$

for

$$A = E_T^{v(1)} E_T^{v(2)} + \vec{\mathbf{p}}_T^{v(1)} \cdot \vec{\mathbf{p}}_T^{v(2)}. \tag{60}$$

Note that the unbalanced solution is simply given by the unconstrained minimum of $M_T^{(a)}$, and for a fixed set of visible and invisible masses the balanced solution is bounded above at

$$A = E^{v(1)} E^{v(2)} + q^{v(1)} q^{v(2)}. \tag{61}$$

In fact, if we take an adequate number of events, we can always find some event which corresponds to such an upper bound [4]. Since we are interested in the M_{T2}^{bal} equal to its own upper bound, we henceforth assume that A is understood as Eq. (61) unless there arises any confusion. Here $\left(E^{v(a)}\right)^2 = \left(q^{v(a)}\right)^2 + \left(m_v^{(a)}\right)^2$ and $q^{v(a)}$ is the magnitude of the total momentum of visible particles seen in the rest frame of their mother particle. The explicit expression for $q^{v(a)}$ can be easily determined in terms of the masses of mother, visible, and invisible particles as follows:

$$q_v^{(a)} = \frac{1}{2M}\sqrt{\left\{\left(M + m_v^{(a)}\right)^2 - \left(m_i^{(a)}\right)^2\right\}\left\{\left(M - m_v^{(a)}\right)^2 - \left(m_i^{(a)}\right)^2\right\}}. \tag{62}$$

One thing to be emphasized is that the dependence of the M_{T2} variable on the effective invisible/DM mass $m_i^{(a)}$ first appear in $q_v^{(a)}$. In other words, M_{T2} is an implicit function of $m_i^{(a)}$ via $q_v^{(a)}$ as mentioned before. Furthermore, we include the possibility that multiple (massive) invisible

---

[44]If the total invariant masses of visible states in both decay chains are the same, only the balanced solutions arise. The reason is because the unconstrained minima for both M_T are identical, there is no possibility that the kinematic configuration like the right panel of Fig. 18 is made. As an example, if there exists only one massless visible particle in each decay chain, the M_{T2} values are always given by the balanced solution.

particles are emitted in each decay chain unlike the previous studies (which considered the cases with two invisible particles having non-identical masses). Hence $m_i^{(a)}$ as well as $m_v^{(a)}$ have their own range once multiple visible and invisible particles are involved in the given decay process. For off-shell intermediate particles the respective ranges are given by (See, for example, [39])

$$\sum_\alpha m_\alpha^{v(a)} = m_{v,\,\text{min}}^{(a)} \le m_v^{(a)} \le m_{v,\,\text{max}}^{(a)} = M - \sum_\beta m_\beta^{i(a)} \tag{63}$$

$$\sum_\beta m_\beta^{i(a)} = m_{i,\,\text{min}}^{(a)} \le m_i^{(a)} \le m_{i,\,\text{max}}^{(a)} = M - \sum_\alpha m_\alpha^{v(a)}. \tag{64}$$

The lower limit corresponds to the situation in which particles described by $p_\alpha^{v(a)}\left(p_\beta^{i(a)}\right)$ are at rest in their center of mass frame so that they move with the same velocity in any frame. The upper limit corresponds to the situation in which particles described by $p_\beta^{i(a)}\left(p_\alpha^{v(a)}\right)$ are at rest in the overall center of mass frame of the final state described by $p_\alpha^{v(a)}$ and $p_\beta^{i(a)}$.

A.2 The Maximum Balanced and Unbalanced M_{T2} Solutions

For the decay with visible/invisible multi-particle final states, it is obvious that balanced/unbalanced M_{T2} solutions have their own range due to the existence of the range in either $m_v^{(a)}$ or $m_i^{(a)}$ or both of them. As far as the upper edge in the M_{T2} distribution is concerned, either the maximum balanced or the maximum unbalanced solution appears as the global maximum. For unbalanced solution, one can easily derive the following relationship from Eqs. (59) and (63).

$$M_{T2}^{\max,unbal} = \tilde{m} + \max\left[m_{v,\text{max}}^{(1)},\, m_{v,\text{max}}^{(2)}\right] \tag{65}$$

For balanced solution, however, it is not easily seen which values of $m_v^{(a)}$ and $m_i^{(a)}$ ($a = 1,\, 2$) will form the maximum balanced solution because of the complication in the corresponding expression $\left(M_{T2}^{bal}\right)^2$ given in Eq. (58). In order to identify those values, we are required to carefully investigate the functional behavior of $\left(M_{T2}^{bal}\right)^2$ according to the changes in $m_i^{(a)}$ and $m_v^{(a)}$, which will be considered in order.

A.2.1 The Change in $m_i^{(a)}$

To see the dependence of $\left(M_{T2}^{bal}\right)^2$ on $m_i^{(1)}$, we simply take the partial derivative:

$$\frac{\partial\left(M_{T2}^{bal}\right)^2}{\partial\left(m_i^{(1)}\right)^2} = \frac{D}{2X\sqrt{B^3 C}} \tag{66}$$

where

$$B \equiv 2A - \left(m_v^{(1)}\right)^2 - \left(m_v^{(2)}\right)^2, \quad C \equiv A^2 - \left(m_v^{(1)}\right)^2\left(m_v^{(2)}\right)^2, \quad X \equiv \sqrt{B + 4\tilde{m}^2} \tag{67}$$

$$D \equiv (BC' - B'C)X^2 + 2A'\sqrt{B^3 C}X + B'BC \tag{68}$$

with the following notations:

$$A' \equiv \frac{\partial A}{\partial \left(m_i^{(1)}\right)^2}, \quad B' \equiv \frac{\partial B}{\partial \left(m_i^{(1)}\right)^2} = 2A', \quad C' \equiv \frac{\partial C}{\partial \left(m_i^{(1)}\right)^2} = 2AA'. \tag{69}$$

One can easily see that A, B, and C are always positive for any set of $m_v^{(a)}$ and $m_i^{(a)}$, and that only positive X is allowed by construction. Also, one can easily prove that A' is negative.

The solutions to $D = 0$ are given as follows:

$$X_1 = -\frac{\sqrt{BC}}{A - \left(m_v^{(1)}\right)^2} \tag{70}$$

$$X_2 = -\frac{\sqrt{BC}}{A - \left(m_v^{(2)}\right)^2}. \tag{71}$$

For $m_v^{(1)} \neq m_v^{(2)}$ it can be proven that either $A - \left(m_v^{(1)}\right)^2$ or $A - \left(m_v^{(2)}\right)^2$ must be positive and the other is positive or negative depending on the parameter space formed by $m_v^{(1)}$ and $m_v^{(2)}$ [4]. Hence, one of the two solutions given above must be negative, which is unphysical, the other is either physically allowed or not. Actually, it turns out that the signs of $A - \left(m_v^{(1)}\right)^2$ and $A - \left(m_v^{(2)}\right)^2$ are connected to the coefficient of X^2 in D in the following way:

$$BC' - B'C = 2A' \left(A - \left(m_v^{(1)}\right)^2\right)\left(A - \left(m_v^{(2)}\right)^2\right). \tag{72}$$

Let us assume that $m_v^{(1)}$ is larger than $m_v^{(2)}$. In this case, $A - \left(m_v^{(2)}\right)^2$ is always positive, i.e., X_2 is always unphysical. Since $A' < 0$ as mentioned above, if $A - \left(m_v^{(1)}\right)^2$ is positive as well, then D, which is a quadratic function in X, becomes a parabola bounded above, and the two solutions X_1 and X_2 all are negative, i.e., unphysical. Therefore, $D < 0$ for arbitrary (physically-allowed) X or $\tilde{m}$. On the other hand, if $A - \left(m_v^{(1)}\right)^2$ is negative, then D turns into a parabola bounded below, and X_1 becomes a physically allowed solution. Therefore, $D < 0$ for $0 < X < X_1$ and $D > 0$ for $X > X_1$. However, in [4] it was shown that X_1 gives rise to

$$M_{T2}^{bal}(X = X_1) = \tilde{m} + m_v^{(1)}, \tag{73}$$

which is simply the unbalanced solution for $m_v^{(1)} > m_v^{(2)}$. Moreover, they showed that this implies that X_1 corresponds to the boundary between the balanced domain and the unbalanced domain. In other words, with X being larger than X_1 the balanced solution is reduced to the unbalanced solution. One can make the same argument and lead the same conclusion for the opposite configuration, i.e., $m_v^{(1)} < m_v^{(2)}$. Also, the dependence on $m_i^{(2)}$ can be easily checked by following similar arguments. Based on hitherto observations, we have

$$\frac{\partial \left(M_{T2}^{bal}\right)^2}{\partial \left(m_i^{(a)}\right)^2} \quad < \quad 0 \tag{74}$$

$$M_{T2}^{\max,bal} \quad = \quad M_{T2}^{bal}\left(m_i^{(1)} = m_{i,\min}^{(1)}, \, m_i^{(2)} = m_{i,\min}^{(2)}\right) \tag{75}$$

for any set of $m_v^{(a)}$ ($a = 1,\ 2$).

A.2.2 The Change in $m_v^{(a)}$

The early work on the dependence of $\left(M_{T2}^{bal}\right)^2$ on $m_v^{(a)}$ was made in [4]. Here we simply provide the final results and mention some modification from the original expression.

$$\frac{\partial\left(M_{T2}^{bal}\right)^2}{\partial\left(m_v^{(a)}\right)^2} \quad \begin{cases} \leq 0 & \text{for } \tilde{m} < m' \\[2ex] \geq 0 & \text{for } \tilde{m} \geq m' \end{cases} \tag{76}$$

$$M_{T2}^{\max,bal} \quad = \quad \begin{cases} M_{T2}^{bal}\left(m_v^{(1)} = m_{v,\min}^{(1)},\ m_v^{(2)} = m_{v,\min}^{(2)}\right) & \text{for } \tilde{m} < m' \\[2ex] M_{T2}^{bal}\left(m_v^{(1)} = m_{v,\max}^{(1)},\ m_v^{(2)} = m_{v,\max}^{(2)}\right) & \text{for } \tilde{m} \geq m'. \end{cases} \tag{77}$$

Here the "kink" location m' can be identified as the true dark matter mass m_{DM} if only a single type of DM is involved [4]. However, in general, it differs from m_{DM} because we do not restrict our consideration to the case with one single-typed DM emitted in each decay chain. Therefore, its expression is written in terms of all parameters (i.e., M, $m_v^{(a)}$, and $m_i^{(a)}$), and it can be calculated by solving the following equation [4]:

$$\sqrt{B + 4m'^2} = \frac{\sqrt{BC}(1 - 2\bar{A})}{2\bar{A}\left(A - (m_v^>)^2\right) + A - (m_v^<)^2} \tag{78}$$

where $m_v^>$ and $m_v^<$ denote the heavier and the lighter (invariant) visible masses between the two decay sides, respectively, and $\bar{A}$ is defined as

$$\bar{A} = \frac{\partial A}{\partial\left(m_v^>\right)^2}. \tag{79}$$

A.3 Discussions and Application

It is a well-known fact that there arises a "kink" in the $M_{T2}^{\max}$ as a function of the trial mass once there exist more than one visible particle in each decay chain and its location is at $\tilde{m} = m_{DM}$ for the cases with a single identical DM particle per decay chain. For more extended case, i.e., $m_i^{(1)} \neq m_i^{(2)}$, one can simply solve Eq. (78). In turns out, however, that this is not the only way of obtaining the kink location. An alternative and simpler way is to find the intersecting point between the maximum balanced and unbalanced solutions. In other words, the solution to satisfy Eq. (78) also satisfies the relation $M_{T2}^{\max,bal} = M_{T2}^{\max,unbal}$. For simplicity, let us assume that $m_{v,\max}^{(1)} > m_{v,\max}^{(2)}$. We then have

$$\left(M_{T2}^{\max,unbal}\right)^2 = \left(\tilde{m} + m_{v,\max}^{(1)}\right)^2 \tag{80}$$

and

$$\left(M_{T2}^{\max,bal}\right)^2 = \tilde{m}^2 + A + \sqrt{\frac{C}{B}\left(B + 4\tilde{m}^2\right)} \tag{81}$$

54

where A is evaluated at $m_i^{(a)} = m_{i,\min}^{(a)}$ as discussed before. Letting Eqs. (80) and (81) be equated and doing some tedious algebra, one can end up with

$$A^2 = \left(m_v^{(1)}\right)^2 \left(m_v^{(2)}\right)^2, \tag{82}$$

which is valid only with $m_v^{(a)}$ being their maximum. Note that $M_{T2}^{\max,bal}$ at $\tilde{m} = m'$ arises when $m_v^{(a)} = m_{v,\max}^{(a)}$ from Eq. (77). Hence, the above-given relationship holds, and the location of the kink can be evaluated by finding the intersection between the maximum balanced and unbalanced solutions.

This observation, actually, leads us to the expressions for $M_{T2}^{\max,bal}$ and $M_{T2}^{\max,unbal}$. Note that it was proven that the balanced solution contributes to the upper edge of the M_{T2} distribution at $\tilde{m} < m'$ in [4]. Also, it is straightforward to prove that the maximum unbalanced solution is larger than the maximum balanced solution at $\tilde{m} \geq m'$. Therefore, as long as the values to give the upper edge of the M_{T2} distribution are concerned, it can be (effectively) understood that the maximum balanced solutions occur at $m_v^{(a)} = m_{v,\min}^{(a)}$ and $m_i^{(a)} = m_{i,\min}^{(a)}$ and the maximum unbalanced solutions do at the maximum of the two $m_{v,\max}^{(a)}$ ($a = 1,\ 2$) for any $\tilde{m}$. As an example, if all visible particles are assumed massless, the maximum balanced and unbalanced solutions are given as follows:

$$M_{T2}^{\max,bal} = \sqrt{\frac{\left(M^2 - m_{i,\min}^{(1)2}\right)\left(M^2 - m_{i,\min}^{(2)2}\right)}{4M^2}} + \sqrt{\frac{\left(M^2 - m_{i,\min}^{(1)2}\right)\left(M^2 - m_{i,\min}^{(2)2}\right)}{4M^2} + \tilde{m}^2} \tag{83}$$

$$M_{T2}^{\max,unbal} = \tilde{m} + \max\left[m_{v,\max}^{(1)}, m_{v,\max}^{(2)}\right] = \tilde{m} + M - \min\left[m_{i,\min}^{(1)}, m_{i,\min}^{(2)}\right] \tag{84}$$

Obviously, the upper edge in the M_{T2} distribution is determined by the maximum value among many events for a given trial DM mass.

$$M_{T2}^{\max}(\tilde{m}) = \max_{\text{many events}}\left[M_{T2}(\tilde{m})\right] \tag{85}$$

Based on the above-discussed understanding, one could expect that taking the maximum between $M_{T2}^{\max,bal}$ and $M_{T2}^{\max,unbal}$ will result in the same value as the above-given Eq. (85).

$$M_{T2}^{\max} = \max\left[M_{T2}^{\max,bal}, M_{T2}^{\max,unbal}\right] \tag{86}$$

It turns out, however, it is true only for the case where there exist more than one visible particle on each decay chain. In the case where there is only one visible particle per decay chain, one can prove that the maximum unbalanced solution is less than the maximum balanced solution for any $\tilde{m}$ so that the $M_{T2}^{\max}$ is simply governed by the $M_{T2}^{\max,bal}\left(m_i^{(a)} = m_{i,\min}^{(a)}\right)$.

B The Existence of a Kink in $M_{T2}^{\max}$ Versus $\tilde{m}$

As discussed in the App. A, it is obvious that for the cases where there is only a single visible particle in each decay chain, the $M_{T2}^{\max}$ as a function of the trial DM mass behaves like a smoothly
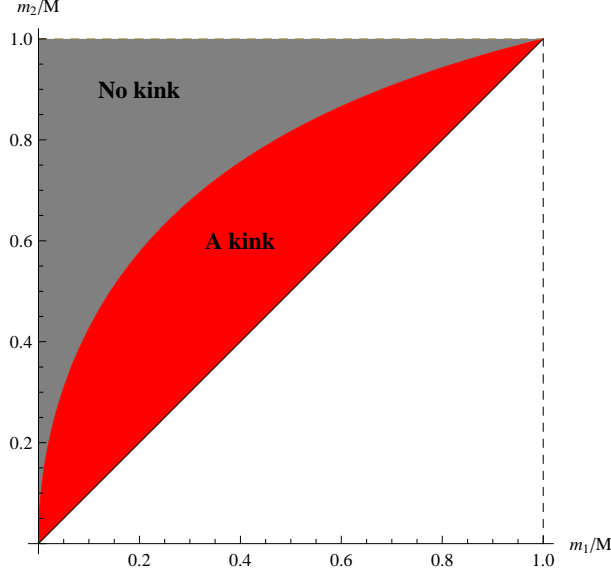
Figure 19: The kinematic regions to have a kink or no kink in the graph of $\frac{m_2}{M}$ versus $\frac{m_1}{M}$.

increasing curve because the upper edge is solely governed by the "balanced" solution in Eq. (58). However, if there exist more than one visible particle per decay chain, the competition between the "balanced" and the "unbalanced" solutions, which is explicitly given in Eq. (86), gives rise to the possibility of a kink (i.e., no longer smooth) in the plot of $M_{T2}^{\max}$ versus $\tilde{m}$. In fact, this approach, the competition between the two types of solutions, enables us to examine easily whether or not there exists a "kink" on the function of the location of $M_{T2}^{\max}$.

In order to have a kink in $M_{T2}^{\max}$ as a function of $\tilde{m}$, the two functions of the maximum balanced and unbalanced solutions over the trial DM mass, i.e., $M_{T2}^{\max,bal}(\tilde{m})$ and $M_{T2}^{\max,unbal}(\tilde{m})$, must cross each other. From Eqs. (58) and (59) they are monotonic functions in $\tilde{m}$, and the slope of Eq. (58) is not greater than that of Eq. (59)($= 1$) over the entire range. These two observations tell us that once a cross-over is made, no additional cross-overs are made. Therefore, it is sufficient to check whether or not the relative sizes of their corresponding functional values at $\tilde{m} = 0$ and $\tilde{m} \to \infty$ are flipped for ensuring such a cross-over. Let us assume that the visible particles are massless for simplicity.[45] From Eqs. (83) and (84) one can easily prove that $M_{T2}^{\max,unbal}$ is larger than $M_{T2}^{\max,bal}$ at $\tilde{m} \to \infty$, and thus $M_{T2}^{\max,bal}$ should be larger than $M_{T2}^{\max,unbal}$ at $\tilde{m} = 0$ to obtain a kink. Their functional values at $\tilde{m} = 0$ are expressed as follows:

$$M_{T2}^{\max,bal}(\tilde{m} = 0) \quad = \quad \sqrt{\frac{(M^2 - m_1^2)(M^2 - m_2^2)}{M^2}} \tag{87}$$

$$M_{T2}^{\max,unbal}(\tilde{m} = 0) \quad = \quad M - m_1 \tag{88}$$

where $m_{i,\min}^{(1)} \equiv m_1$ and $m_{i,\min}^{(2)} \equiv m_2$, and we assumed $m_1 \leq m_2$ without loss of generality. Therefore,

_____

[45]One can easily apply the same argument for the case of massive visible particles.

56

the condition to have a kink is simply given by

$$\sqrt{\left(1 - \frac{m_1^2}{M^2}\right)\left(1 - \frac{m_2^2}{M^2}\right)} > 1 - \frac{m_1}{M}, \tag{89}$$

which can be further simplified to

$$\frac{m_1}{M} < \frac{m_2}{M} < \sqrt{\frac{2m_1}{M + m_1}}. \tag{90}$$

Likewise, one can easily find the condition to have no kink as follows:

$$\frac{m_2}{M} > \sqrt{\frac{2m_1}{M + m_1}}. \tag{91}$$

Fig. 19 shows the regions for a kink or no kink pictorially; the red area represents all possible kinematic configurations for the existence of a kink while the gray one all possible kinematic configurations for no kink. Elsewhere is not physically allowed due to the assumption that $m_1 \le m_2$.

There is a special case where each decay chain emits only one *single*-typed DM particle, i.e., $m_1 = m_2$. The Z_2 models or the E_2 type events of Z_3 models belong to this case. The range to satisfy Eq. (91), i.e., the condition to have no kink, is $\frac{m_1}{M} > 1$ or $\frac{m_1}{M} < -2$ both of which are not physically allowed. Therefore, we always obtain a kink in $M_{T2}^{\max}$ as a function of the trial DM mass as expected [4].

As another concrete example, let us take E_3 type events of Z_3 models, where one of the two decay chains emits a single dark matter particle whereas the other one emits two dark matter particles with intermediate particles *off*-shell. Like before, we assume that all DM particles to be emitted in the full decay process have the same mass so that the *minimum* of the effective dark matter mass of the two DM side to give the maximum balanced solution is $m_{DM}^{eff} = 2m_{DM}$, i.e., $m_1 = m_{DM}$ and $m_2 = 2m_{DM}$. From Eqs. (90) and (91) the conditions to have a kink or no kink are more simplified to

$$\text{A kink:} \quad 0 < \frac{m_{DM}}{M} < \frac{\sqrt{3} - 1}{2} \tag{92}$$

$$\text{No kink:} \quad \frac{\sqrt{3} - 1}{2} < \frac{m_{DM}}{M} < 1, \tag{93}$$

which was mentioned in Sec. 3.2 and demonstrated in Fig. 4.

C Algorithm to Find the Upper Edge of M_{T2} Distribution

In this appendix, we describe an algorithm to identify the $M_{T2}^{\max}$ for events after the R_{P_t} cut. As we discussed in section 5.1.1, in Z_3 models where there is only one visible particles per decay chain, and the visible particles in the decay chains with one DM and two DM are identical, the total

M_{T2} distribution becomes a combination of the distributions of E_2 and E_3 events. So the idea is to apply an R_{P_t} cut (a cut on the ratio of P_t's of visible particles on the two decay chains in the same event) to "remove" the E_2 events. This in principle can give us a relatively pure sample of E_3 events, which has a smaller $M_{T2}^{\max}$. But in practice/reality, there is still a small number of E_2 events that survive the R_{P_t} cut. Therefore, the upper edge of M_{T2} distribution for events after the R_{P_t} cut is hard to be determined due to the "contamination" of E_2 type events. This is shown in the right panel of Fig. 8, which shows clearly that there are small number of events which has M_{T2} beyond the $M_{T2}^{\max}$ of E_3 type events. Here we propose an algorithm to identify/extract the "would-be" $M_{T2}^{\max}$ for E_3 events by removing E_2 contamination events and then do a fitting to the resulting distribution.

First, we need to "subtract" the contaminating events. To do this, we calculate the moving average of the number of events per bin including the last n bins in the M_{T2} distribution: A_n. The choice of moving average makes this quantity rather stable under statistical fluctuations as we increase n. However, as we increase n to the point below $M_{T2}^{\max}$ for E_3 type events, we start to get a sharp rise on A_n. Based on this, we define $n_{\max}$ to be the bin such that $A_{n_{\max}+1} \geq 2.5 A_{n_{\max}}$. This bin is considered as a rough separation point between "contaminating" E_2 type events and the start of E_3 type events. And we treat $A_{n_{\max}}$ as a rough estimate for the E_2 type events contribution to the number of events per bin.

Next, we pick events with $n > n_{\max}$ and subtract $A_{n_{\max}}$ from the number of events in each bin. This gives us an approximate M_{T2} distribution for pure E_3 type events. Since we do not have an analytical formula for the M_{T2} distribution for E_3 type events, we can only do a fitting for events near and to the left of the bin $n_{\max}$ to find the upper edge of the M_{T2} distribution. We choose two fitting functions, one linear function and one quadratic function, and did the fitting separately. Our final answer for the $M_{T2}^{\max}$ is given by the average of the values obtained by these two fitting methods, and their difference is regarded as the error due to fitting.